

Short Title of the Project: **SELF-STARTING SOLID-STATE LASER
WITH DYNAMIC SELF-ADAPTIVE CAVITY**

**Final Report To European Office of Aerospace Research and Development
(Years 2001-2002)**

Name of Organization: Institute of Applied Physics (IAP) of the Russian Academy of Science (RAS).

Principal Investigator: Oleg Antipov

Full home address: 4 "1" avenue Kazansky, apartment 23, Nizhny Novgorod, 603000 Russia; home telephone: +7(8312) 192642.

Office address: 46 Uljanov St., Nizhny Novgorod, 603950 Russia, IAP RAS; office telephone: +7(8312) 384547; fax: +7(8312) 363792.

E-mail: antipov@appl.sci-nnov.ru

Date of completion: July 5, 2002

REPORT DOCUMENTATION PAGE

Form Approved OMB No. 0704-0188

Public reporting burden for this collection of information is estimated to average 1 hour per response, including the time for reviewing instructions, searching existing data sources, gathering and maintaining the data needed, and completing and reviewing the collection of information. Send comments regarding this burden estimate or any other aspect of this collection of information, including suggestions for reducing the burden, to Department of Defense, Washington Headquarters Services, Directorate for Information Operations and Reports (0704-0188), 1215 Jefferson Davis Highway, Suite 1204, Arlington, VA 22202-4302. Respondents should be aware that notwithstanding any other provision of law, no person shall be subject to any penalty for failing to comply with a collection of information if it does not display a currently valid OMB control number.

PLEASE DO NOT RETURN YOUR FORM TO THE ABOVE ADDRESS.

1. REPORT DATE (DD-MM-YYYY) 04-10-2002			2. REPORT TYPE Final Report	3. DATES COVERED (From – To) 27-Nov-00 - 27-May-02	
4. TITLE AND SUBTITLE Self-Starting Solid-State Laser With Dynamic Self-Adaptive Cavity			5a. CONTRACT NUMBER ISTC Registration No: 1913p		
			5b. GRANT NUMBER		
			5c. PROGRAM ELEMENT NUMBER		
6. AUTHOR(S) Dr. Oleg Antipov			5d. PROJECT NUMBER		
			5d. TASK NUMBER		
			5e. WORK UNIT NUMBER		
7. PERFORMING ORGANIZATION NAME(S) AND ADDRESS(ES) Institute of Applied Physics 46 Uljanov Str., Nizhny Novgorod 603600 Russia			8. PERFORMING ORGANIZATION REPORT NUMBER N/A		
9. SPONSORING/MONITORING AGENCY NAME(S) AND ADDRESS(ES) EOARD PSC 802 BOX 14 FPO 09499-0014			10. SPONSOR/MONITOR'S ACRONYM(S)		
			11. SPONSOR/MONITOR'S REPORT NUMBER(S) ISTC 00-7018		
12. DISTRIBUTION/AVAILABILITY STATEMENT Approved for public release; distribution is unlimited.					
13. SUPPLEMENTARY NOTES					
14. ABSTRACT <p>This report results from a contract tasking Institute of Applied Physics as follows: The present project is directed at the development of physical principles of creation of solid-state lasers of a new class with cavity completed by dynamic holographic gratings induced in a nonlinear medium by generating beam itself. The self-starting laser oscillator based on Nd:YAG laser crystals with cavity formed with participation of refractive-index and gain gratings accompanied by population gratings induced in the laser crystal by generating waves will be studied both experimentally and theoretically.</p> <p>The industry-related importance of our project is indicated in its main goal: the solution of a very important problem of laser engineering, that is the creation of a high power industrial laser with good beam quality. Such lasers could find numerous applications in precision technologies such as drilling of small apertures, cutting, spot thermo-hardening of metals, treatment of ceramics and other materials.</p>					
15. SUBJECT TERMS EOARD, Physics, Optics					
16. SECURITY CLASSIFICATION OF:		17. LIMITATION OF ABSTRACT UL	18. NUMBER OF PAGES 30	19a. NAME OF RESPONSIBLE PERSON Alexander J. Glass, Ph. D.	
a. REPORT UNCLAS	b. ABSTRACT UNCLAS	c. THIS PAGE UNCLAS		19b. TELEPHONE NUMBER (Include area code) +44 (0)20 7514 4953	

TABLE OF CONTENTS

	PAGE
I. MAIN SCIENTIFIC RESULTS OF THE PROJECT	3
1. Spectroscopic investigations of population of the high-energy levels in Nd-containing laser crystals and glasses	4
1.1. Fluorescence of Nd:YAG and Nd:YAP crystals under laser pumping	4
1.2. Study of fluorescence of Nd:YAG crystal under combined diode and laser pumping	7
2. Interferometric investigation of the refractive-index changes in the Nd:YAG crystal under diode and laser pumping	9
2.1. Results of interreferometric measurements in Nd:YAG laser crystal under diode pumping	10
2.2. Results of interferometric measurements of RIC in Nd:YAG laser crystal under combined diode and laser pumping	12
3. Investigations of the self-starting laser oscillator with cavity completed by a single grating	14
4. Investigation of spectra and temporal dynamics of the self-starting oscillator	15
5. Numerical modeling of the self-starting lasers	17
6. Influence of phase nonreciprocity of the dynamic cavity on the oscillation condition of the holographic laser	18
6.1. Numerical study of dynamic laser with nonreciprocal cavity	18
6.2. Experimental study of the self-starting laser with phase-nonreciprocal cavity	20
7. Investigation of mode-locking in self-starting laser with dynamic cavity.	21
7.1. Self-starting laser with a non-Bragg multi-grating nonlinear mirror	21
7.2. Mode-locking in laser with a double-phase conjugate mirror in the fast nonlinear absorber	22
8. Experimental investigation of the high average power laser	23
9. References	27
II. Presentation of the results	28
III Purchase of the equipment	29
IV Budget report	30

I. MAIN SCIENTIFIC RESULTS OF THE PROJECT

1. Fluorescence spectra of several Nd³⁺-containing laser crystals (Nd:YAG and Nd:YAP) and laser glass Nd:ZBLAN under intensive diode pumping (at 808 nm), laser pumping (at 266 nm, 354 nm and 532 nm) and their combination were investigated at wavelengths of 370-650 nm. Several fluorescence lines caused by transition from the high-energy level $^2F(2)_{5/2}$ were registered. An effective channel of population of the $^2F(2)_{5/2}$ level by a two-step transition was found. In Nd:YAG crystal it was: the first step is the transition from the ground state to metastable level $^4F_{3/2}$ under diode pumping, the second step is an 4f-5d intershell transition from the $^4F_{3/2}$ level to the $^2F(2)_{5/2}$ level (through 5d electron shell) under fourth harmonic pumping.
2. Refractive index changes in Nd:YAG laser crystals under intensive diode pumping (at 808 nm), laser pumping (at 266 nm) and their combination were studied by a sensitive polarization Jamin-Lebedev interferometer. The thermal and electron components of the index changes were separated. The value of the electron component caused by different polarizability of excited and unexcited Nd³⁺ ions was determined. The electron changes of the refractive index were found to be comparable with the thermal component in a Nd:YAG rod under QCW diode pumping (at 808 nm) with pulse duration of 200 μ s. The electron component predominated in Nd:YAG under combined diode pumping and the fourth-harmonic laser pumping (at 266 nm).
3. Self-starting conditions of a flash-lamp-pumped Nd:YAG laser oscillator with dynamic holographic mirror were experimentally studied for different cavity architectures. The oscillation threshold in the cavity completed by a long-period grating was found to be lower than that of a laser with cavity completed by a small-scale grating. This effect was explained by a larger number of fluorescence components, which jointly induce the population grating.
4. The dynamics of the generating wave in the self-starting Nd:YAG laser with a cavity formed by population grating was investigated. The probability of the single-mode regime was found to be high enough near oscillation threshold of the self-starting laser. The stability of the single-longitudinal mode generation reduced with an increase in pumping power. The probability of single-longitudinal mode generation was found to be higher in the laser with cavity completed by the long-period grating in comparison with the cavity completed by the small-period grating.
5. The spatio-temporal model of the self-starting oscillator was numerically calculated for different models of the random noise source: distributed delta-correlated (in-space and time) noise, and in-boundary localized noise. The oscillation dynamics were qualitatively similar for the two-noise model; however, the self-oscillation threshold was found slightly lower for localized noise. The oscillation threshold decreased in the presence of several longitudinal modes when all modes formed a single grating.
6. The influence of phase nonreciprocity of the cavity completed by the population grating on the self-starting oscillation was studied both experimentally and numerically. The oscillation threshold decreases in the laser with cavity with $\pi/2$ phase nonreciprocity in comparison with the reciprocal laser cavity.
7. The possibility of self-starting oscillation in Nd:YAG laser with cavity completed by population grating induced by a fast-relaxed saturable absorber was studied. The generation of a mode-locking pulse train in the self-starting laser was realized.
8. Different schemes of the high-average-power laser with dynamic cavity completed by holographic grating were studied. The generation of the good-quality beam with average power of 200W was obtained in the laser based on two flash-lamp pumped Nd:YAG rods of big sizes $\varnothing 12 \times 135$ mm. The additional improvement of beam quality was obtained by an additional polarization rotator and telescope image transfer from the principal plane of one rod to the principal plane of the other rod. The scheme was found to be scaleable for increase of power of the beam with good quality.

1. Spectroscopic investigations of population of the high-energy levels in Nd-containing laser crystals and glasses

In our previous study, a very important role of the quasi-metastable level $^2F(2)_{5/2}$ in explaining the origin of the strong nonlinearity of the Nd-containing laser crystal has been demonstrated (Fig. 1.1). This high-energy level has great polarizability at near-IR wavelengths, and mainly determines the electron index changes in flash-lamp pumped Nd:YAG [1,2]. In the frame of this project the population of this level under laser and diode pumping was studied by fluorescence spectroscopy.

EXPERIMENTS: A Nd:YAG or Nd:YAP rod (4 mm in diameter) and a Nd:ZBLAN sample were pumped by the second, third or fourth harmonics of an additional Q-switched Nd:YAG laser (at 532 nm, 354.7 nm or 266 nm, respectively) in combination with a CW diode bar array or QCW diode stack (at 808 nm) (Fig. 1.2). Pulse duration of the Nd:YAG laser was about 10 ns, repetition rate was 10...14 Hz. Pulse energy was up to 10 mJ at the second harmonic; up to 0.5 mJ and 2 mJ at the third and fourth harmonics, respectively; up to 20 W for the CW laser diode bar array; and up to 300 W in pulse for QCW diode stack. The optical beam of the CW diode bar array was chopped and synchronized with pulses of the harmonics. The size of the pumped area in the Nd:YAG crystal was $10 \times 0.1 \text{ mm}^2$ and $10 \times 0.2 \dots 0.4 \text{ mm}^2$ for the harmonics and laser diode beam, respectively.

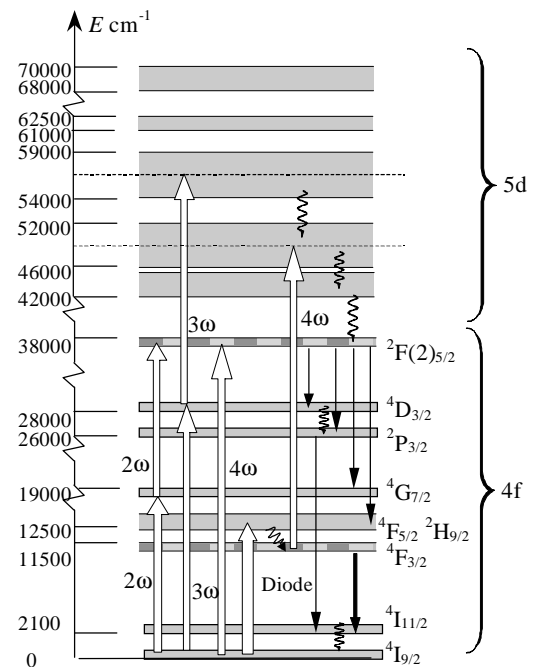


Fig. 1.1. Electron energy levels of Nd^{3+} ions in Nd:YAG laser crystal.

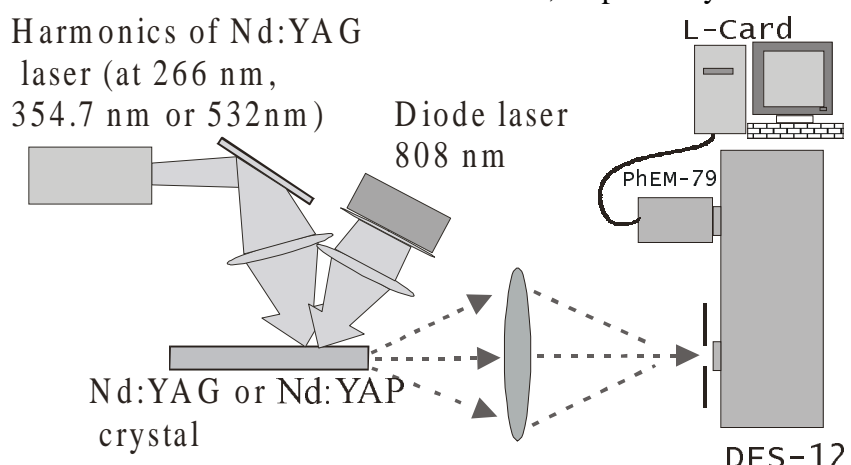


Fig. 1.2. Experimental schematic of spectroscopic study of fluorescence of laser crystals pumped by laser diode bar array, and the second, third or fourth harmonics of an additional pulsed Nd:YAG laser.

The fluorescence signal (in the wavelength range of 370-650 nm) was detected by a monochromator and a photodetector, filtered and amplified by a differential amplifier (which was synchronized with laser pulses), and calculated by a computer.

1.1. Fluorescence of Nd:YAG and Nd:YAP crystals under laser pumping

The registered fluorescence signal contained several spectrum lines which corresponded to transitions from the $^2(F2)_{5/2}$ electron level (Fig. 1.3). This identification was made based on

information about energy position of the levels inside the 4f-electron shell of the Nd:YAG laser crystal [3,4], and previous results of fluorescence measurements in the Nd:YAG crystal under laser pumping [5,6]. The fluorescence band at 400.5 nm (of the transition from the $^2F(2)_{5/2}$ level to the $^2H_{9/2}$ level) was chosen to indicate the population of the level $^2F(2)_{5/2}$. The luminescence intensity at this spectrum line was measured to be quadratically dependent on the second-harmonic intensity and linearly on the fourth-harmonic intensity even in the absence of the diode pump (Fig. 1.4). This result showed the possibility of two-photon transition to the $^2F(2)_{5/2}$ level from the ground state $^4I_{9/2}$ (through the intermediate state of $^4G_{7/2}$) induced by the second harmonic (at 532 nm) and of a single-step excitation of the $^2F(2)_{5/2}$ level induced by the fourth harmonic (at 266 nm) (Fig. 1.1). This result is in good agreement with previously published studies [5-7].

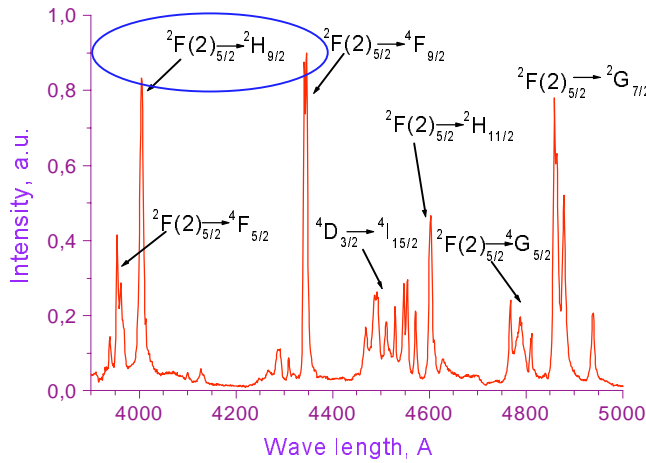


Fig. 1.3. Fluorescence spectra of Nd:YAG crystal at pumping of 266 nm or 532 nm.

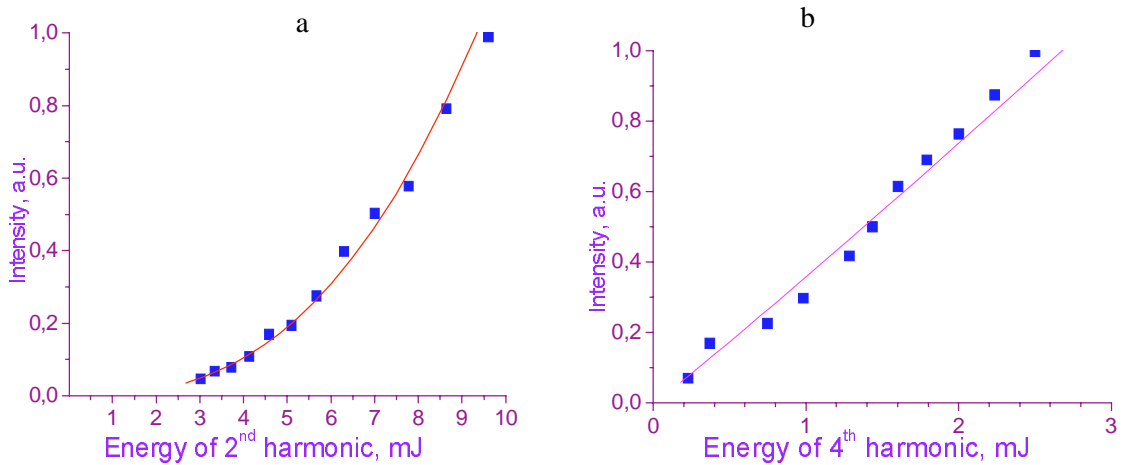


Fig. 1.4. Fluorescence intensity at 400.5 nm of Nd:YAG crystal under pumping at 532 nm (a) and at 266 nm (b).

The measured spectrum of the visible fluorescence under third-harmonic pumping (at 354 nm) can be explained by transitions from $^4D_{3/2}$ and $^2P_{3/2}$ levels of Nd³⁺ ions. This result is also in good qualitative agreement with previous experimental results of several groups [5,6]. However, we have obtained several new results. The fluorescence spectra of Nd:YAG crystal measured under pumping at the third harmonic of Nd:YAG laser was found to be dependent on the pump energy. Under the pump energy $E_p \leq 0.2$ mJ the spectral lines were identified to be transitions $^4D_{3/2} \rightarrow ^4I_{13/2}$, $^2P_{3/2} \rightarrow ^4I_{11/2}$, and $^4D_{3/2} \rightarrow ^4I_{15/2}$, $^2P_{3/2} \rightarrow ^4I_{13/2}$ (Fig. 1.5). The increase of the third harmonic pulses energy leads to appearance of new fluorescence lines that correspond to transitions from $^2F(2)_{5/2}$ level to $^4F_{5/2}$, $^2H_{9/2}$ and $^4F_{9/2}$. The fluorescence intensity was measured to be quadratically dependent

on the optical pump energy. Such kind of dependence of the fluorescence lines can be explained by two-step population of this level when Nd^{3+} ions are excited through the $^4\text{D}_{3/2}$ level to the level of 5d-electron shell (after absorption of the second photon of the third harmonic), and then by nonradiative transition from 5d-levels to the $^2\text{F}(2)_{7/2}$ and $^2\text{F}(2)_{5/2}$ levels. The UV broad-band fluorescence at 380 nm may be explained by 5d-4f radiation transitions directly from the levels of the 5d-electron shell.

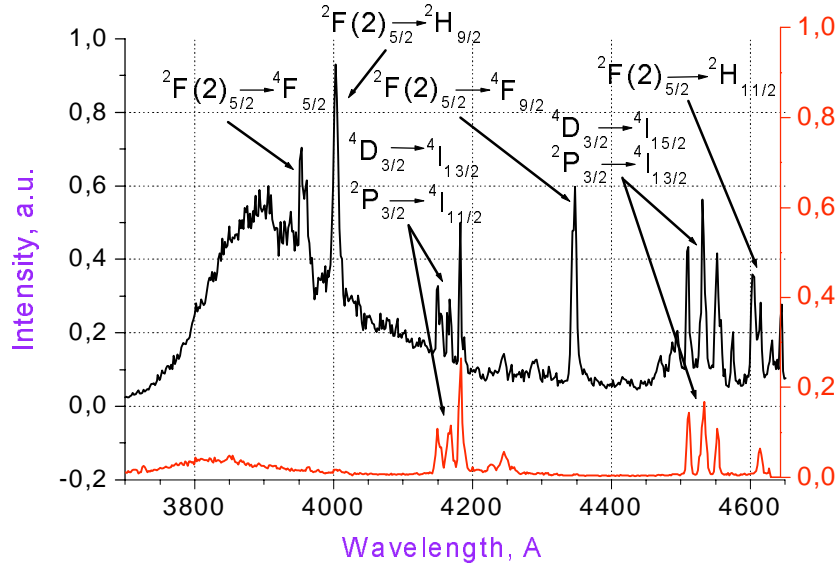


Fig. 1.5. Fluorescence spectra of Nd:YAG under third-harmonic pumping at 354.7 nm with pulse energy 0.2 mJ (red curve) and with pulse energy of 0.5 mJ (black curve).

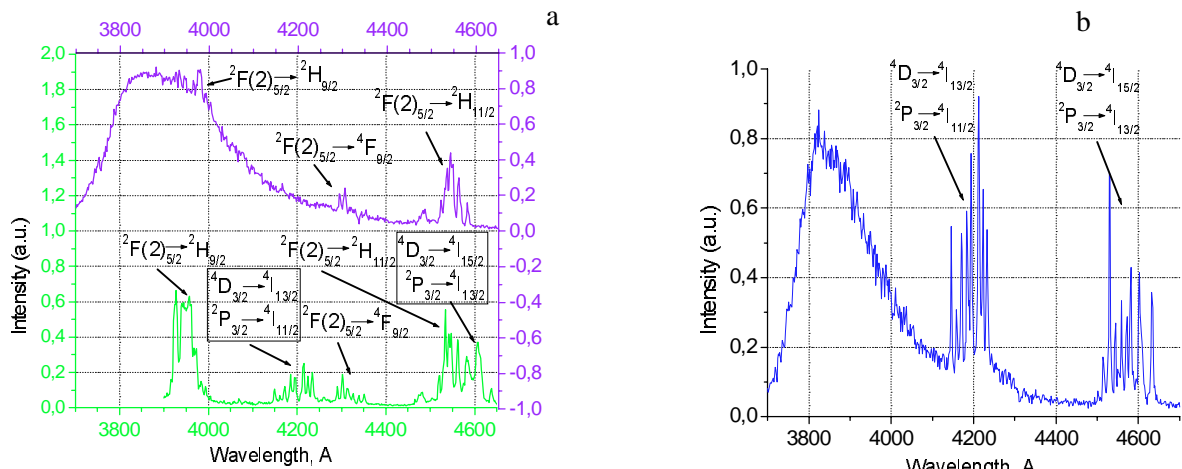


Fig. 1.6. Fluorescence spectra of Nd:YAP under fourth-harmonic pumping at 266 nm (a - violet curve) or second-harmonic pumping at 532 nm (a - green curve) and third-harmonic pumping at 354.7 nm (b).

The fluorescence spectra in Nd:YAP pumped at 532 nm and 266 nm consist of lines which can be explained by transitions from the $^2\text{F}(2)_{5/2}$, $^4\text{D}_{3/2}$ and $^2\text{P}_{3/2}$ levels of Nd^{3+} ions (Fig. 1.1). Note, that these spectra differ from fluorescence spectra of Nd:YAG crystal under the same pumping. An explanation to these differences is in the difference in absorption of the crystal matrixes: the population of the $^2\text{F}(2)_{5/2}$ level due to 266 nm pumping of Nd:YAP is more difficult in comparison with Nd:YAG because of strong absorption of the YAP matrix (beginning at about 300 nm) (Fig. 1.6a). Under the third harmonic pump (at 354.7 nm) of Nd:YAP crystal, the fluorescence at several

lines corresponding to $^4D_{3/2} \rightarrow ^4I_{13/2}$, $^2P_{3/2} \rightarrow ^4I_{11/2}$, $^4D_{3/2} \rightarrow ^4I_{15/2}$ and $^2P_{3/2} \rightarrow ^4I_{13/2}$ transitions was registered (Fig. 1.6b). The energy of these lines is close to that in Nd:YAG crystal.

Interesting fluorescence measurement results were obtained in Nd-containing fluorozirconate glass (Nd:ZBLAN) pumped by the second, third and fourth harmonics of an additional Nd:YAG at wavelengths of 532 nm, 354 nm, and 266 nm, respectively. The host glass composition was (in mol. %) 53ZrF₄-20BaF₂-4LaF₃-3AlF₃-20Na (ZBLAN). The simplest interpretation of the luminescence spectrum can be made for the case of the third-harmonic-pumped Nd:ZBLAN at 354.7 nm. The key point is the absorption transition from the ground state $^4I_{9/2}$ to the $^4D_{3/2}$ level [8]. This level is quite metastable (in Nd:YAG its life time is about 2.2 ns). So, the visible luminescence spectra can be explained by transitions from this $^4D_{3/2}$ level and $^2P_{3/2}$ (the latter is populated by radiationless relaxation from the directly-excited $^4D_{3/2}$ level). The luminescence spectrum of Nd:ZBLAN pumped by the second harmonic (at 532 nm) has additional lines in the violet-blue spectral range: at 395 nm, 460 nm, and 470 nm (this spectrum can be explained by transitions from the $^4G_{7/2}$ level (direct pumping), the $^2F(2)_{5/2}$ level (two-step excitation), and the $^4D_{3/2}$ level). The luminescence spectrum of Nd:ZBLAN pumped by the fourth harmonic (at 266 nm) has a broadband violet line (this spectrum can be explained by transitions from the $^2F(2)_{5/2}$ level, which is populated by direct transition from the ground state).

1.2. Study of fluorescence of Nd:YAG crystal under combined diode and laser pumping

The fluorescence spectra of Nd:YAG and Nd:YAP crystals were studied by combined pulsed laser pumping and pumping by a CW diode array or QCW diode stack (at 808 nm). The experiments showed that the higher-lying levels are much stronger populated by the pumping beam at 266 nm (or 532 nm) in the presence rather than in the absence of diode pumping (compare red and blue curves in Fig. 1.7). Fluorescence intensity at 400.5 nm pumped by the 266-nm beam increased by an order of magnitude in the presence of the CW diode-pumping in comparison with no diode pumping (Fig. 1.8). Interestingly, this increase was observed when power of the diode beam at 808 nm was about 10^{-5} in comparison with the fourth-harmonic power.

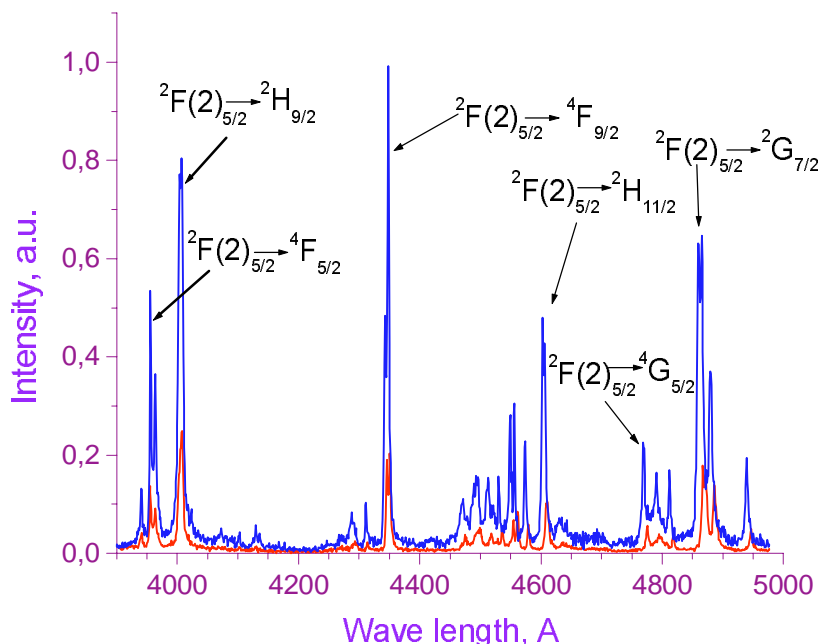


Fig. 1.7. Fluorescence spectra of Nd:YAG crystal under laser pumping at 266 nm (red) and combined pumping at 266 nm and 808 nm (blue).

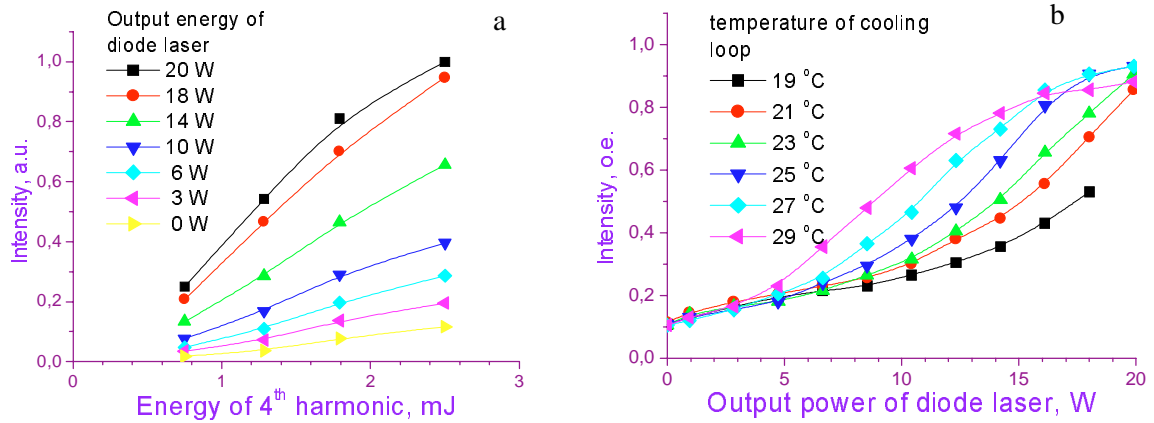


Fig. 1.8 Fluorescence intensity of Nd:YAG crystal at 400.5 nm under combined pumping by diode (at 808 nm) and 4-th harmonic (at 266 nm) vs diode pumping power (a) and energy of the 4-th harmonic pulse (b).

The fluorescence in Nd:YAG laser crystal was studied also using a QCW laser-diode stack at 808 nm (produced by “JENOPTIK Laserdiode GmbH”) with pulse duration of 200...250 μ s and peak power up to 300 W. Additional pumping by fourth harmonics of a pulsed Nd:YAG laser (with pulse duration of 10 ns) was also used (the harmonic pulse was time-synchronized with the end of the diode-stack pulse).

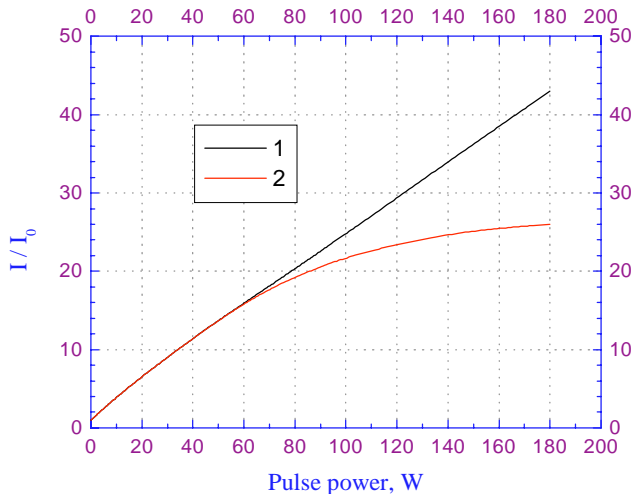


Fig. 1.9. Fluorescence intensity of Nd:YAG crystal at 400.5 nm under combined pumping by QCW diode stack (at 808 nm, pulse duration is $\tau \sim 200 \mu$ s) and 4-th harmonic (at 266 nm, $\tau \sim 10$ ns, pulse energy is $E=2$ mJ) vs pulse power of the diode stack (1 – with control of wavelength, 2 – without control of wavelength).

In diode-pumped Nd:YAG with additional 4-harmonic pumping (at 266 nm) the visible fluorescence was measured to have the same spectrum as in the previous investigation with CW pumping (see Fig. 1.7). The measured spectrum indicates radiation transitions from the $^2F(2)_{5/2}$ level. The fluorescence power increased almost linearly with an increase in the diode power under optimization of the pump frequency varied by varying the diode temperature (black curve in Fig. 1.9). The fluorescence power increased by more than 40 times in the presence of the QCW diode pumping in comparison with the case when there is no diode. (Fig.1.9). The fluorescence was clearly seen by the human eye.

The strong increase of fluorescence at 400.5 nm is explained by population of the $^2F(2)_{5/2}$ level induced by the fourth harmonics due to two-step transition through the $^4F_{3/2}$ level (the latter level was populated, in turn, from the ground state by the laser diode beam). The 266-nm wave induces the strong (well-allowed) transition from the populated $^4F_{3/2}$ level to the 5d electron shell, then the 4f-5d inter-shell radiationless relaxation (with a characteristic time of 2 ns [7]) provided the population of the $^2F(2)_{5/2}$ level (through the $^2F(2)_{7/2}$ level) (Fig 1.1). This channel of the $^2F(2)_{5/2}$ level population appears to be the main one because of the strong well-allowed inter-shell 4f-5d

transition whose cross-section is two orders of magnitude more than for the low-allowed intra-shell 4f-4f transitions.

The strong violet fluorescence in Nd:YAG under the combined pumping may offer a possibility of lasing at 435 nm or 400.5 nm. However, our first attempt to obtain generation at 400.5 was unsuccessful, probably due to strong spontaneous emission at 1064 nm, which decreases the population of the ${}^4F_{3/2}$ level.

It should be noted that the visible fluorescence intensity both in Nd:YAG and Nd:YAP crystals under third-harmonic pumping (at 354 nm) was found to be practically independent of the diode pumping at 808 nm. Moreover, the visible fluorescence in Nd:YAP crystal under pumping by the second or fourth harmonics was measured to be independent of additional diode pumping at 808 nm (at least up to 20W of the CW-diode pumping).

Note, that in Nd:YAG we did not register any visible fluorescence (at 370...600 nm) under single QCW diode pumping with pulse power up to 300 W (only the well-known IR lines were registered).

2. Interferometric investigation of the refractive-index changes in the Nd:YAG crystal under diode and laser pumping

The problem of interferometric measurements of refractive index changes (RIC's) in Nd:YAG laser crystal under diode and laser pumping was solved using a compact Jamin-Lebedev polarization interferometer (Fig. 2.1). Two testing cross-polarized optical beams from a stable He-Ne laser (with output power up to 5 mW at 633 nm) propagated inside one Nd:YAG rod 9 mm in length and 5 mm in diameter. One testing beam propagated through an area inside the Nd:YAG rod which was pumped by a QCW-diode stack at 808 nm (or a diode stack in combination with the fourth harmonic of Nd:YAG laser at 266 nm) (Fig. 2.2). The other propagated through a non-pumped area of the Nd:YAG rod.

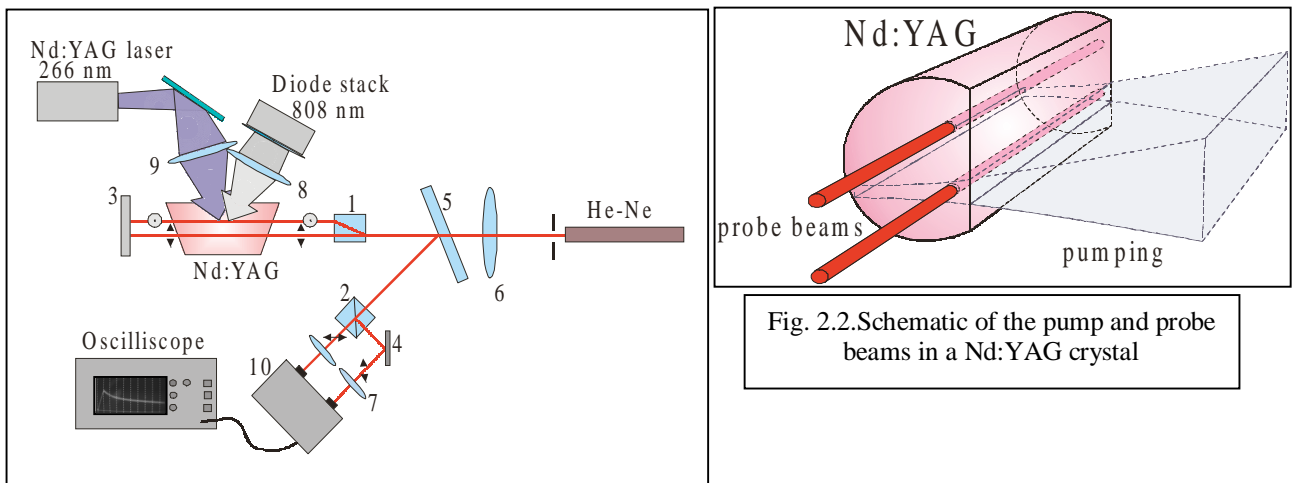


Fig 2.1. Schematic of the polarization interferometer, 1 – polarization beam splitter, 2 – Glan prism, 3,4 – TR-mirrors, 5 – semi-reflected mirror, 6, 7, 8, 9 – lenses, 10 – two channel receiver with an electronic differential amplifier

To reduce noise in the interferometer a two-channel receiver with differential electronic amplifier (number 10 in Fig. 2.1) was used. The noised signals of random fluctuations due to mechanical vibrations or luminescence were deducted by the differential amplifier with the two-channel receiver. To decrease the luminescence at laser wavelength the right end of the Nd:YAG rod has a mirror-reflecting coating at 1064 nm. So the sensitivity of the interferometer to the phase-shift difference was increased to 2×10^{-6} . Signal-to-noise ratio in the working point of the interferometer was more than 5×10^2 .

2.1. Results of interreferometric measurements in Nd:YAG laser crystal under diode pumping.

The changes of refractive index of Nd:YAG laser crystal under diode pumping were registered by an interferometer setup. The pulse duration of the diode stack (at 808 nm) was about 200...250 μ s, the peak power was varied up to 250 W. The pumping beam (with divergence $1^\circ \times 10$ when collimated by a cylindrical lens) was focused additionally onto the Nd:YAG crystal by a spherical lens with focal length varied from 5 cm to 15 cm.

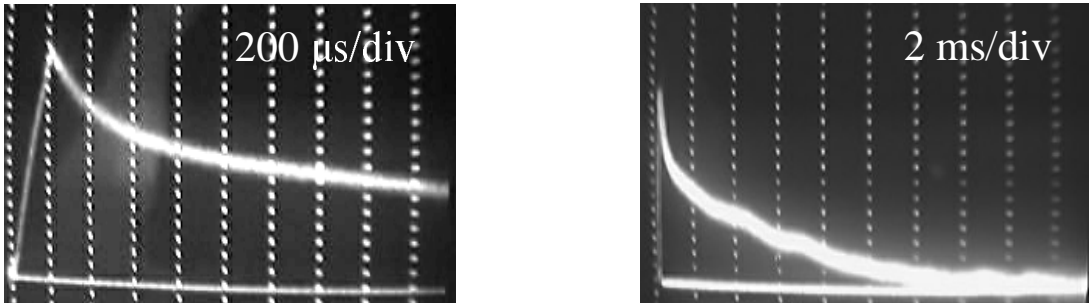


Fig. 2.3. Oscillograms of the interferometric signal of Nd:YAG under QCW diode pumping (with pulse duration of 200 μ s)

Oscillograms of the RIC's indicate their linear increase during pumping pulse (Fig. 2.3). Two-exponential decay after the end of the pumping pulse was registered (Fig. 2.3 and Fig. 2.4). The slow decay (component A_2 in the approximation given in Fig. 2.4) with characteristic time varied with varying focusing length from 3...4 ms to 6...7 ms can be identified with relaxation of thermally-induced changes of refractive index. The fast decay component ($\sim A_1$ in the approximation given in Fig. 2.4) has characteristic time of about 250 μ s that was found to be independent of the focusing lens. This decay time corresponds to lifetime of the metastable level $^4F_{3/2}$ of the working laser transition of the Nd:YAG crystal. For these reasons this component can be identified with the “electronic” changes of the refractive index due to different polarizability of the ground state $^4I_{9/2}$ and the excited metastable level $^4F_{3/2}$.

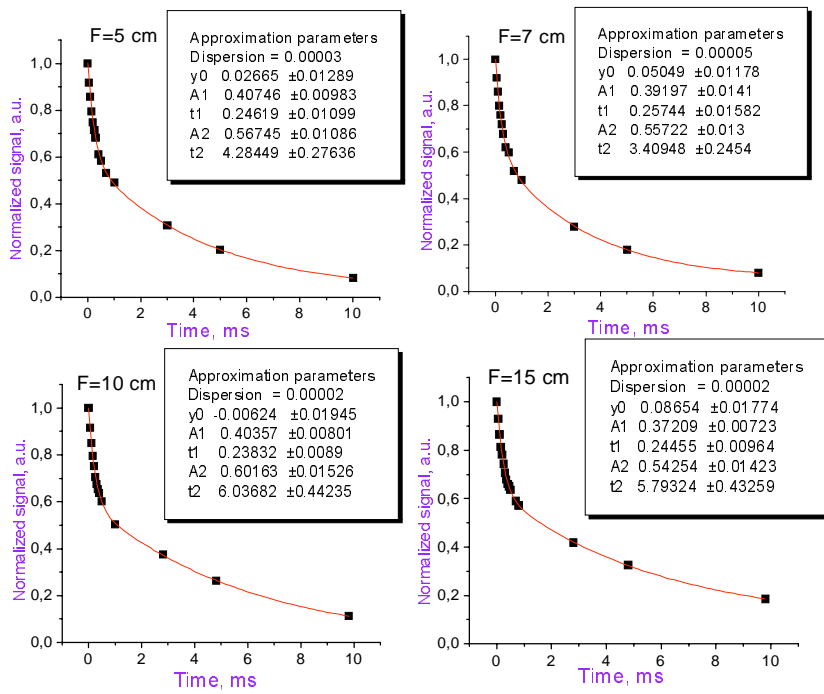


Fig.2.4. Approximation of interferometric signal (for different lenses used to focus the diode pumping beam) by formula $Y=Y_0+A_1 \times \exp(-t/t_1)+A_2 \times \exp(-t/t_2)$
The first exponent is the electronic RIC, the second is the thermally induced RIC.

An analytical approximation of the relaxation of the index changes by two exponents has shown that the “thermal” and “electronic” components are comparable for all focusing lenses used (Fig. 2.4). The ratio of the “thermal” and “electronic” components was also independent of the diode pumping power. This fact is in good accord with the given explanation of the origin of the RIC components. Indeed, both the thermal and electronic changes of the refractive index must grow proportionally to fluence of the pumping pulses with duration of about 200 μ s.

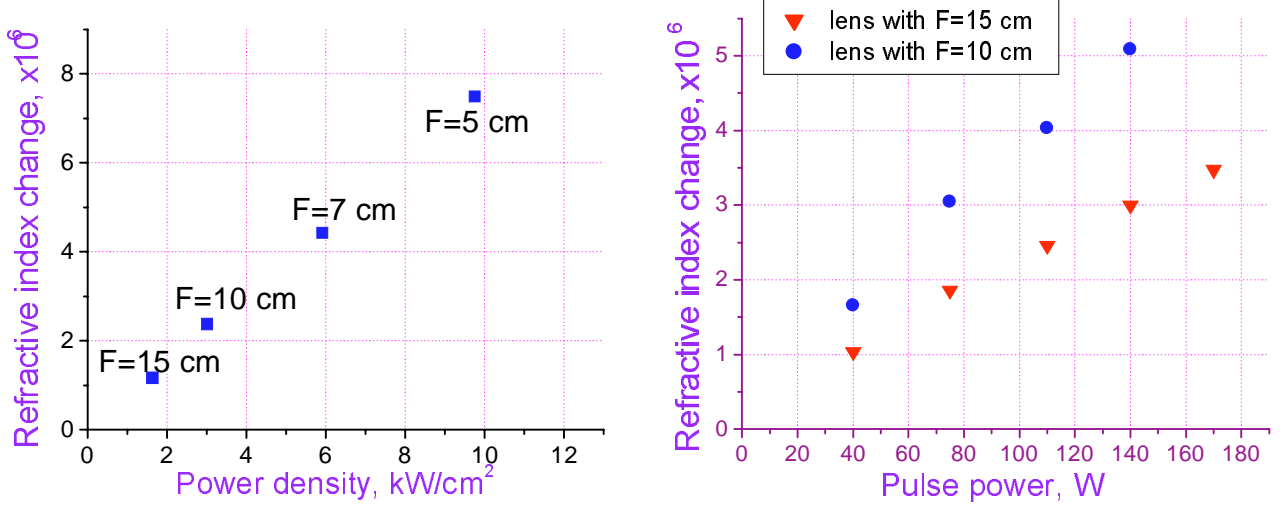


Fig. 2.5. Dependencies of the refractive index changes on pumping intensity for fixed pumping power (a) and on pumping power (b) for different spherical lenses focusing the diode-stack beam into Nd:YAG crystal; F is the focal length of the lens.

The interferometric experiment allowed us to determine absolute values of the RIC's. The total RIC increased up to $1\dots2\times10^{-5}$, the maximal “electronic” RIC was about 5×10^{-6} . We know from previous spectroscopic measurements that the $^4F_{3/2}$ level is populated mostly by the diode pumping, and population of other higher levels was small [1 R5]. Taking into account that only the $^4F_{3/2}$ level is excited and using the measured value of RIC (Δn) it is possible to estimate its population (N_F) by formula:

$$N_F = \frac{n_0 \Delta n}{2\pi F_L^2 \Delta p}, \quad (2.1)$$

where Δp is the difference of polarizability of the excited level $^4F_{3/2}$ and the ground state $^4I_{9/2}$; $F_L = (n_0^2 + 2)/3$ is the Lorentz factor; n_0 is the refractive index of the Nd:YAG.

If the difference of polarizability of the excited level $^4F_{3/2}$ and the ground state $^4I_{9/2}$ is $\Delta p = 3.9 \cdot 10^{-26} \text{ cm}^3$ (for the Nd:YAG crystal at 630 nm) [2,3 R5], the estimation of the $^4F_{3/2}$ population by expression (1) gives us $N_F \approx 10^{-19} \text{ cm}^{-3}$. It means 20% population of the $^4F_{3/2}$ level for all Nd³⁺ ions in our Nd:YAG crystal with 1% concentration of Nd ($5 \cdot 10^{19} \text{ cm}^{-3}$).

Small-signal amplification at $\lambda=1.064 \mu\text{m}$ in the diode-pumped Nd:YAG crystal was directly measured (Fig 2.6a). The result of the gain measurement allows us to determine the population of the excited level $^4F_{3/2}$ (N_F) by formula:

$$N_F = \frac{\ln(I_{out} / I_{in})}{2\sigma l}, \quad (2.2)$$

where $\sigma = 3.5 \cdot 10^{-19} \text{ cm}^2$ is the gain cross-section at $\lambda=1.064 \mu\text{m}$, $l = 0.6 \text{ cm}$ is the pumping length, I_{out} and I_{in} are the output and input intensities of the optical beam.

The determined populations of the excited $^4F_{3/2}$ level from the interferometric measurements (by formula 2.1) and the gain measurement (by formula 2.2) under the same pumping were approximately the same (Fig. 2.6b). This fact indicates the high reliability of the RIC determination.

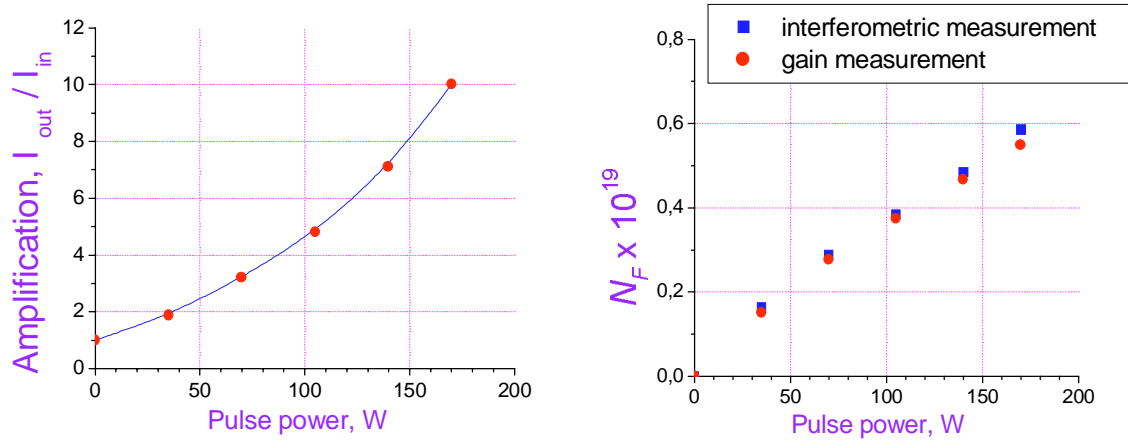


Fig. 2.6. Amplification at $\lambda=1.064 \mu\text{m}$ in the Nd:YAG crystal (a) and approximations of the population of the metastable $^4F_{3/2}$ (b) vs pulse power of a QCW diode laser at 808 nm.

Therefore, the interferometric measurements showed that the “electronic” component of RIC in Nd:YAG laser crystal under QCW diode pumping is comparable with the “thermal” RIC.

2.2. Results of interferometric measurements of RIC in Nd:YAG laser crystal under combined diode and laser pumping.

A next step in our investigation was the interferometric measurements of the RIC’s in Nd:YAG laser crystal under combined pumping by a laser beam and the diode stack. The fourth-harmonic of the pulsed Nd:YAG laser (at a wavelength of 266 nm) was used for this additional pumping. Our previous spectroscopic investigations showed two-step excitation of the quasi-metastable higher-lying level $^2(F2)_{5/2}$ under combined diode and laser pumping at wavelengths of 808nm and 266nm, respectively [1 R5]. Therefore, similar pumping was used to excite the RIC.

The interferometric measurement showed a small RIC in the Nd:YAG crystal under a single pulse (with duration of about 10 ns) of the fourth-harmonic pumping at 266 nm. The slow relaxation dynamics of the RIC indicates the thermal origin of the effect.

The RIC was registered to be stronger under the combined pumping in comparison with the single diode pumping and the single fourth-harmonic pumping. The two pumping beams at 808nm and 266nm co-propagated in the volume of Nd:YAG crystal (the experimental scheme was shown in Fig. 2.1). The pulse energy at 266 nm was varied up to 2mJ, pumping power of a pulse from the diode-stack at a wavelength of 808 nm was up to 250W. The 10-ns pulse of the fourth harmonic was varied in time with respect to the diode-pumping pulse with duration of 200...250 μs . The strongest RIC was registered when the fourth-harmonic pulse corresponded to the end of the diode-pumping pulse.

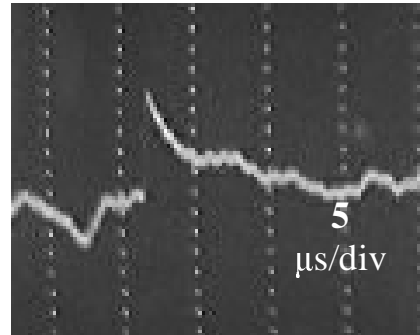


Fig. 2.7. Oscillogram of interferometric signal in a Nd:YAG amplifier under combined diode (at $\lambda=808 \text{ nm}$, $\tau=200 \mu\text{s}$) and laser pumping by 4-th harmonic of Nd:YAG (at $\lambda=266 \text{ nm}$, $\tau \sim 10 \text{ ns}$)

Again, the dynamics of the RIC relaxation indicates two components: slow-relaxed thermal component and fast component with decay time of about 3 μ s (Fig 2.7). The latter “electronic” component is explained by population of the $^2F(2)_{5/2}$ level with life time ~ 3 μ s. This fact is in good accord with our previous spectroscopic study. The value of the total RIC induced by the 10-ns fourth-harmonic pulse was very high. We reached saturation of the interferometer when it was in the most sensitive point before any pumping (total interferometric phase shift under diode and laser pumping was more than $\pi/2$). Estimation of the fast “electronic” RIC (induced by the combined pumping) gives us value of $1.2...1.5 \times 10^{-6}$ for quite a small power of diode-stack pulse (20...60 mW) and fourth-harmonics pulse energy 2 mJ (Fig. 2.8a). This RIC is comparable with the total RIC under single diode pumping with the same power and intensity (Fig. 2.5b). The “electronic” RIC for stronger diode power was difficult to determine due to the “interferometer saturation” resulting in fast oscillation of the measured signal.

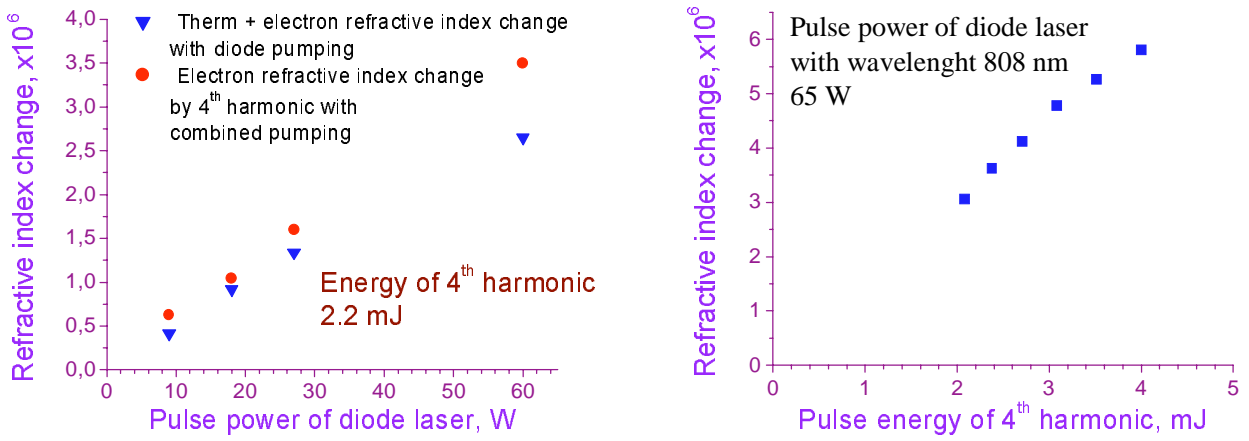


Fig. 2.8. Refractive index changes of Nd:YAG crystal vs pulse energy of 4-th harmonic when the pulse power of QCW diode laser (at 808 nm) is a constant (a) and pulse power of a QCW diode laser when the pulse energy of 4-th harmonic is a constant (b)

The interferometric investigation of Nd:YAG under combined pumping (the diode-stack peak power was increased up to 60W) showed a linear increase of the electronic RIC with increasing fourth-harmonic pulse energy (Fig. 2.8b). The maximum electronic RIC was determined in this experiment to be $\sim 6.0 \times 10^{-6}$, which is much higher than the total RIC in Nd:YAG ($\sim 2.2 \times 10^{-6}$) under single diode pumping with the same power. The linear approximation of the electronic RIC to the high pumping pulse power (for the fixed fourth-harmonic energy of 2.2 mJ) gives $\sim 1.7 \times 10^{-5}$ (at 300 W pulse power of the diode stack).

3. Investigations of the self-starting laser oscillator with cavity completed by a single grating

The experimental investigation of the self-starting laser with cavity completed by single transmission or reflection grating was performed (see also report 1 [9]).

To realize a single reflecting grating or a single transmitting grating we used a scheme of the self-starting oscillator with an additional nonreciprocal device – polarization isolator (PI). This device comprises two counter-rotating Faraday rotators and a polarizer placed between them (Fig. 3.1 and Fig. 3.2). The isolator allowed propagation of only one polarization in each way. As a result, clockwise and anti-clockwise waves in the cavity were orthogonally polarized. The nonreciprocal device provided the self-starting generation in the cavity which was formed by only one grating (the transmitting grating or reflecting grating): 1) two intersecting waves were cross-polarized and did not induce the grating; 2) the backward-reflecting gratings, which were induced by counterrunning

waves, did not contribute to the cavity formation.

Two schemes of the self-starting Nd:YAG laser oscillator were studied in experiment. They differed by the geometry of wave intersection inside the laser crystal and by the period of population gratings induced inside the laser crystal. In the first scheme, nearly counterrunning generated optical waves intersected in the Nd:YAG amplifier and induced the large-scale transmitting grating (TG) of population that can complete the cavity (Fig. 3.1). The $\lambda/4$ plate served as a polarization rotator (PR), which in combination with the mirror provided optical feedback in the cavity.

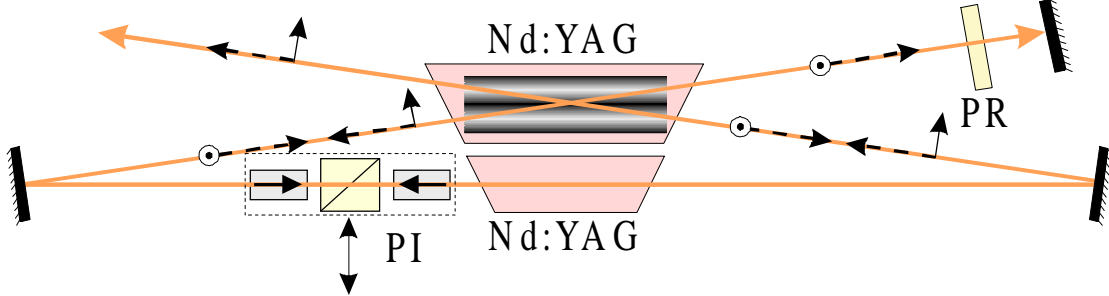


Fig. 3.1. The self-starting laser with cavity completed by the transmitting grating, PI is polarization isolator based on a Faraday rotator, PR is $\lambda/4$ plate.

In the second scheme, nearly co-propagating waves intersected in the laser crystal and induced the small-scale reflecting grating (RG) of the population that can complete the cavity (Fig. 3.2).

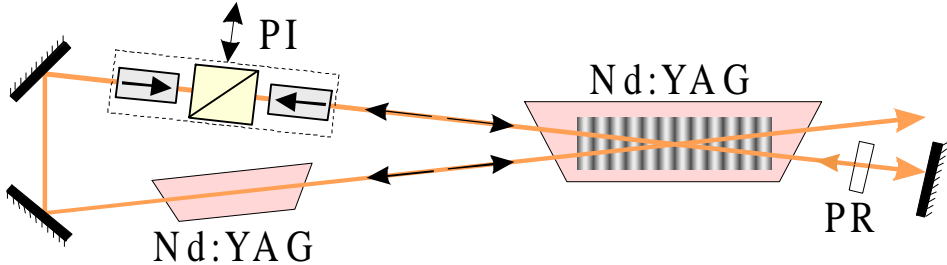


Fig. 3.2. The self-starting laser with cavity completed by the reflecting grating, PI is polarization isolator based on a Faraday rotator, PR is $\lambda/4$ plate.

Either scheme comprised two laser amplifiers with flash-lamp pumped Nd:YAG laser crystals. Nd:YAG laser rods with dimensions of $\varnothing 6 \times 100$ mm or $\varnothing 10 \times 100$ mm were used in the amplifiers. Pulse duration of flash-lamp pumping was about 300 μ s with a repetition rate of about 1-30 Hz.

The experiments showed that generation threshold in the scheme with the large-scale TG is much less than with RG (Fig. 3). The threshold amplification of the intra-loop laser amplifier in scheme 1 (Fig. 1) was found to be much less than the amplification in scheme 2 (Fig. 2). This result confirms that the large-scale transmitting grating induced by a large number of ASE components (much more than in the case of the small-scale reflecting grating) has a stronger amplitude at the pre-generation stage, therefore providing a faster switching and larger intensity of the generation wave.

The obtained result is explained by different spatio-temporal selectivity of the luminescence wave forming the nonlinear dynamic mirror. The self-starting conditions of the laser oscillator with the dynamic cavity can be achieved due to the large intensity of amplified spontaneous emission (ASE). An appropriate level of ASE corresponds to multimode noise within the broadband luminescence line. However, in this explanation, there appears a problem of phase mismatch between optical waves reflected from the gratings that are induced by the different ASE waves within the full luminescence line.

Phase mismatches of the small-scale RGs induced by counterpropagating optical waves at frequencies within the luminescence line (in a nonlinear active rod several centimeters in length) are very big. Therefore, only a small number of luminescence components can participate in the formation of the reflecting grating that completes the cavity. So it is possible to expect large threshold of the self-starting oscillation in the laser-oscillator whose cavity is formed by the RG.

In contrast to the reflecting grating, the phase mismatch of a large-scale TG induced by waves with different wave vectors is significantly less (for the same length of the nonlinear layer). Different optical waves (longitudinal modes) at frequencies within the full luminescence line can participate in the formation of the joint TG. According to our estimations, the ASE intensity provided by the full luminescence line is quite sufficient for the self-consistent initiation of generation. Therefore, threshold of the self-starting oscillation in the laser with a nonlinear mirror formed by the TG appears to be much less than that for the RG.

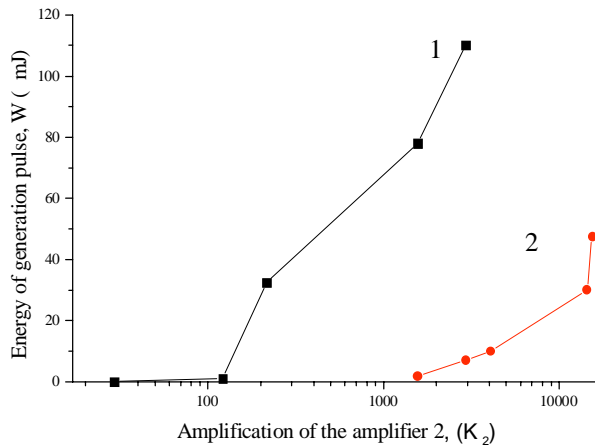


Fig. 3.3. The energy of the generated pulse vs gain of the intra-loop amplifier in schemes with the PI device with TG (curve 1) and RG (curve 2).

Oscillograms of the generation in schemes with TG or RG were slightly different: the dynamics of the generation in the scheme with RG was more chaotic. The existence of pre-generation was observed in both cases.

4. Investigation of spectra and temporal dynamics of the self-starting oscillator

To understand the self-starting conditions of the laser oscillator with a cavity completed by a single holographic grating, the spectrum of longitudinal modes and temporal dynamics of the optical beam near generation threshold were studied simultaneously (see also report 2 [10]).

The study of self-starting oscillators with cavity completed by a single grating (transmitting or reflecting) in the single and double-output scheme was continued. The spectra and temporal dynamics of generated beams were measured simultaneously. The experimental schemes are presented in Fig. 3.1 and Fig. 3.2 for the single-output schemes, and Fig. 4.1 and Fig. 4.2 for the double-output schemes. Again, the single-grating regime was achieved by use of a nonreciprocal device (a polarization isolator).

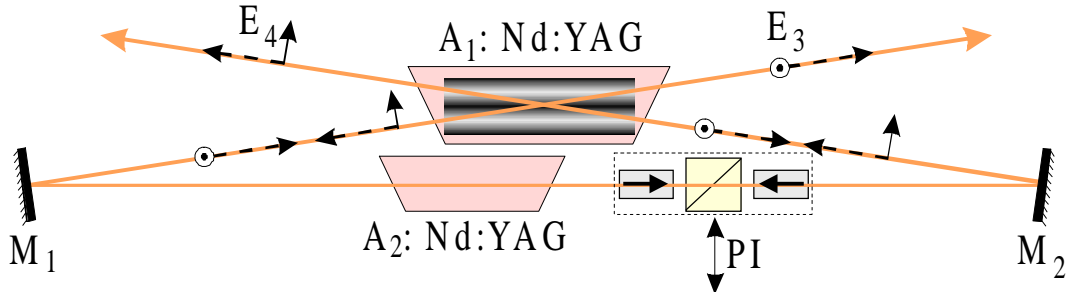


Fig. 4.1 The ring-cavity self-starting laser with a transmitting grating completing the cavity, PI is polarization isolator based on a Faraday rotator.

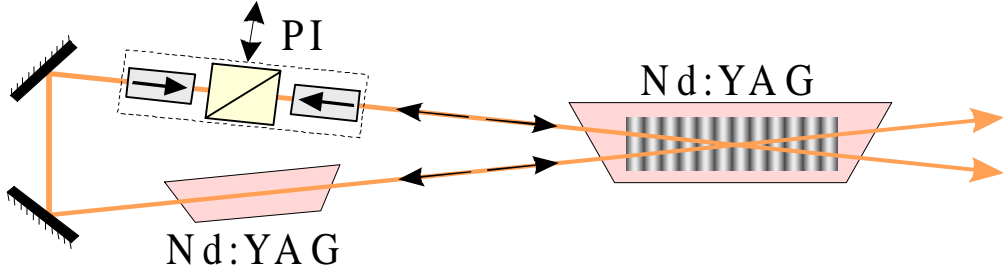


Fig. 4.2. The self-starting laser with a ring cavity completed by RG, PI is polarization isolator based on a Faraday rotator.

EXPERIMENTAL RESULTS: Measurements of temporal dynamics and spectra of longitudinal modes show that the single-mode generation can occur near oscillation threshold in all schemes (with double or single output, with cavity completed by a single long-period transmitting or small-period reflecting grating). However, the probability of the single-mode generation in a scheme of co-propagating strong waves (with the reflecting grating completing the cavity) was measured to be less than in the scheme of counter-propagating strong waves (with the transmitting grating completing the cavity) both for the double- and single-output oscillator (Table 1).

Table 1. Probability of single-mode generation in self-starting lasers near threshold

Number of outputs	Single-output scheme	Double-output scheme
Type of grating that completes the cavity		
Long-period transmitting grating	23 % (schematic is presented in Fig. 3.1)	36 % (schematic is presented in Fig. 4.1)
Small-period reflecting grating	11 % (schematic is presented in Fig. 3.2)	13 % (schematic is presented in Fig. 4.2)

Temporal dynamics of the generated wave both for the single-output and double-output schemes of the self-starting laser with cavity completed by a single long-period transmitting grating were similar. In those schemes, an increase in the longitudinal-mode number correlated with a decrease in delay time of the generated pulse.

In the single-output scheme with the small-period reflecting grating (Fig. 3.2) the probability of single-mode generation was measured to be small (Table 1), and the dynamics of generated pulses in the multi-longitudinal mode regime was registered to be chaotic. This dynamics can be explained by multimode generation during each pulse. This temporal behavior appears to be similar to the free-running generation in an ordinary laser with a linear mirror.

In the double-output scheme with the small-scale reflecting grating (Fig. 4.2, see also report 1 [9]) the probability of the single-mode generation was small again (Table 1), but generated pulses in the multi-longitudinal mode regime were more smooth than in the previous case of the single-output scheme. It can be explained by single-mode generation during each pulse and by the change in the generation frequency from pulse to pulse.

Therefore, the study of the generation spectra and oscilloscopes has shown good discrimination of the longitudinal modes in the case of the cavity completed by the long-period transmitting grating. This fact may be explained by really “nonlinear” self-starting generation when the mode discrimination is determined by both the frequency dependence of gain and the diffraction efficiency of the nonlinear grating. The high generation threshold, the small probability of the single-mode generation in the scheme with the small-period reflecting grating, and the “free-running” oscillation dynamics may be explained by onset of generation due to the “linear” diffuse scattering on rod boundaries, microirregularities and defects of the laser crystal structure. These explanations are in good agreement with our previous study of generation threshold. Indeed, the long-period transmitting grating can be induced (under generation threshold) simultaneously by a large number of spontaneous emission components within the full luminescence line. So, threshold of the “nonlinear” generation in this scheme is low, and above threshold of the self-starting oscillation we have significant narrowing of the generation line due to the dependence of gain on frequency. In the case of co-propagating waves, the possibly-induced small-period grating cannot be strong (under generation threshold), and the generation can start at higher amplifier gain due to “linear” diffuse reflection at rod boundaries and random scattering inside a laser crystal. Our measurement of “linear” random scattering inside the laser crystal indicates such a possibility for high amplifier gain.

5. Numerical modeling of the self-starting lasers

During this project numerical modeling of different schemes of the self-starting lasers was performed. The laser schemes with one or two outputs, with or without cavity nonreciprocities were studied numerically. The sets of the partial derivative equations for electrical field of the optical waves (in the plane wave approximation), average-in-space population and population gratings were calculated. The Euler’s method with different spatio-temporal grids (for example, with crossed grids for electric fields amplitudes and population gratings) was used. Different models of the noise source were assumed (the delta-correlated distributed noise, the equivalent noise in the boundary, the regular population grating inside the active medium).

The self-starting oscillations were obtained in several of the investigated models. However, the generation threshold depended on many factors. For an optical scheme the threshold of the oscillation was different for different models of the initial noise source. The influence of the noise source spectrum on generation threshold was investigated. The generation threshold was found to be dependent on the spectrum of the noise source. The delta-correlated distributed noise source required the longest calculation time, and corresponded to the highest threshold of the self-starting oscillations. Different method of calculations also gave different generation threshold (even for the same noise source).

In the single output scheme of the laser the generation was obtained for all model we used, in the cases of a single grating completing the cavity and multi-gratings cases. The oscillation threshold was little dependent on the number of gratings in the cavity. Several resonances of the frequency detuning (the parameter ΩT_1) of the intersecting intracavity waves were found. The average intensity of the random noise source (the threshold noise for the self-starting laser) was determined $10^{-7} \dots 10^{-5}$.

In the double-output schemes the generation was obtained for the multi-gratings regimes for all used model of the initial noise. However, in the case of a single grating completing the cavity and delta-correlated random distributed noise source the self-starting oscillation was not found.

The existence of a determined grating of population in the active media led to a threshold decrease in the several studied schemes. However, the amplitude of the determined grating was required quite big, and it could not be explained by the real pump distribution inside the active medium. The really existing random pump inhomogeneity can give a contribution to the additional distributed feedback, when the oscillation threshold is quite big. For this reason, the self-starting conditions of the laser on the population gratings can be provided by random spontaneous polarization in the active medium, or random inhomogeneities in the pumped area.

In general, the results of numerical calculations were in an accord with the experimental results. In particular, the necessity of the refractive index gratings in the active medium for the self-starting condition of the dynamic laser with a random noise source was confirmed.

6. Influence of phase nonreciprocity of the dynamic cavity on the oscillation condition of the holographic laser

Two kinds of self-starting laser oscillators with cavity formed by holographic gratings induced in an active medium by generating beams themselves have been studied so far. A group from Imperial College (London) headed by Dr. M.J. Damzen has studied the self-starting oscillator with the cavity formed by gain gratings in the presence of the amplitude and phase nonreciprocity [11]. Another kind of the self-starting laser with a reciprocal cavity completed by refractive-index grating in a laser crystal has been studied by ourselves (see, for example, [12]). The both schemes of the self-starting lasers can be implemented using a Nd:YAG laser crystal. For the nonreciprocal cavity, gain gratings were supposed to play the main role for positive feedback, whereas in the reciprocal cavity moving refractive-index gratings may provide the generation condition.

In this report we present the results of theoretical and experimental investigation of the influence of phase nonreciprocity on characteristics of the self-starting holographic laser based on a Nd:YAG laser crystal with an amplitude-reciprocal cavity. The goal of this study is to verify the theory of the self-starting lasers and search for an optimal scheme of the laser.

6.1 Numerical study of dynamic laser with nonreciprocal cavity

It is known in the theory of phase conjugating oscillators that different kinds of holographic gratings provide a condition for oscillation, and its threshold depends on the reciprocity or nonreciprocity of the cavity. Optimal phase nonreciprocity for a self-pumped phase conjugator based on a refractive-index grating is $\pi/2$; optimal phase nonreciprocity (in the presence of cavity amplitude nonreciprocity) for a gain grating is π . Similar optimal nonreciprocity is for photorefractive materials with gratings of local and non-local origin [13].

A self-starting laser is a more complicated object; however, it is possible to expect that optimal phase and amplitude nonreciprocities of this system may be similar to those of the phase conjugator. Another problem is the complex character of the origin of the nonlinearity of the laser crystal. At least in a flash-lamp pumped Nd:YAG crystal the population gratings are accompanied by both the gain gratings and refractive-index gratings.

A model of the self-starting Nd:YAG laser was numerically investigated by partial derivative equations using Euler's crossed-grids method. The existence of both gain and refractive-index gratings accompanying the population gratings was assumed. Different phase nonreciprocities of the self-starting laser cavity for clockwise and anti-clockwise waves were studied (Fig. 6.1).

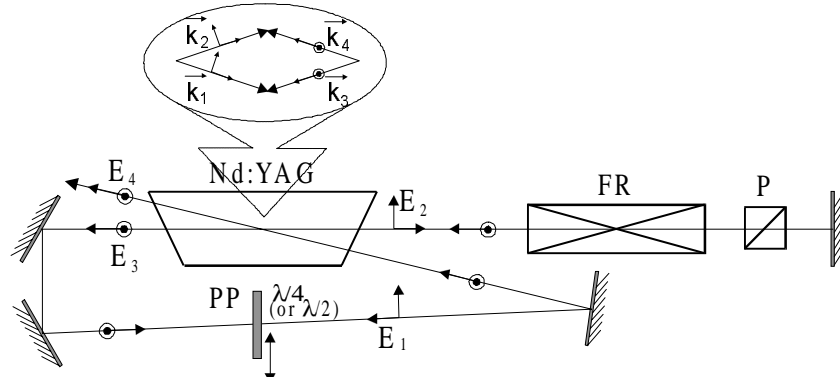


Fig. 6.1. Experimental schematic of the self-starting laser and diagram of wave vectors of generating waves.

Calculations showed that the holographic laser (its generation threshold and the output power) with an amplitude reciprocal cavity is quite sensitive to the phase nonreciprocity (Fig. 6.2). Optimal phase nonreciprocity for the nearest threshold was found to be 1.7π . The biggest difference for the energy of the output pulse train can be achieved for different phase nonreciprocities near the oscillation threshold.

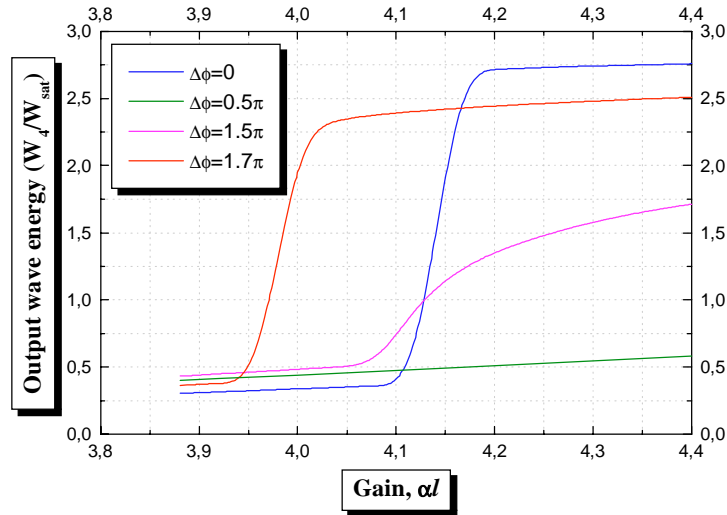


Fig. 6.2. Numerically calculated dependence of the pulse-train energy vs small-signal gain for different values of phase nonreciprocity of the self-starting cavity near the oscillation threshold.

Optimal frequency phase shift was found to be dependent on the phase nonreciprocity. The following figures show the output wave maximum intensity vs intracavity frequency shift for different values of phase nonreciprocity at different noise source intensities (I_n): near the oscillation threshold (Fig. 6.3a, $I_n=1.5\cdot10^{-4}I_{sat}$) and far above the oscillation threshold (Fig. 6.3b, $I_n=5.5\cdot10^{-4}I_{sat}$). The oscillation threshold value is $I_{n\ thres}=1.22\cdot10^{-4}I_{sat}$ without any phase nonreciprocity (with small-signal gain $\alpha l = 4$) and $I_{n\ thres}=9.65\cdot10^{-5}I_{sat}$ with near-optimal phase nonreciprocity.

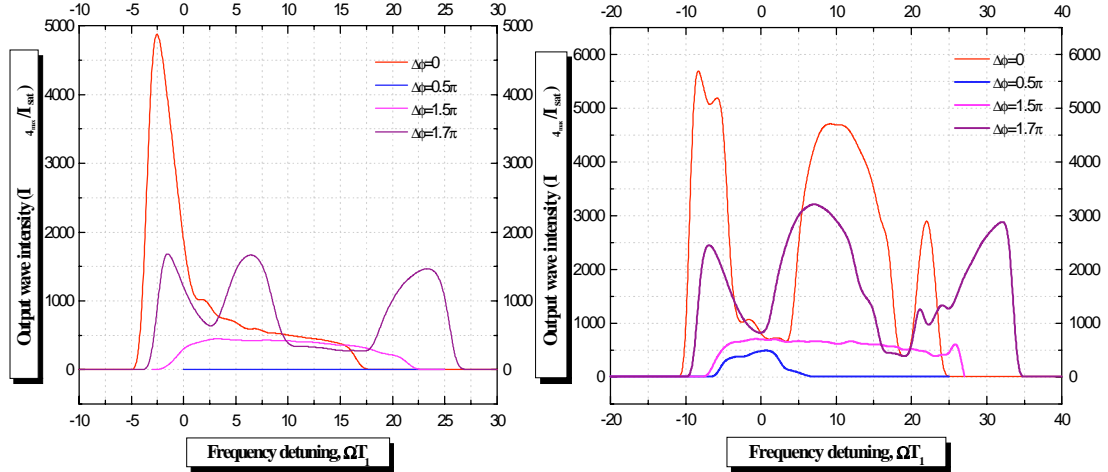


Fig. 6.3. Numerically calculated dependence of the output peak power vs frequency detuning of the generated beam for different values of phase nonreciprocity near (a) and far above (b) oscillation threshold.

6.2 Experimental study of the self-starting laser with phase-nonreciprocal cavity

The phase nonreciprocity of the holographic cavity of the self-starting laser was realized by use of a phase plate ($\lambda/2$ or $\lambda/4$) and orthogonal polarizations of clockwise and anti-clockwise waves (Fig. 6.1). The polarization of the waves in the cavity was determined by a polarizer (P) and a Faraday rotator (FR). Different orientation of the phase plate (PP) allowed us to have the phase nonreciprocity of $\pi/2$, $-\pi/2$, π and $-\pi$. Flash-lamp pumped Nd:YAG amplifiers ($\varnothing 6 \times 10$ -mm rod) were used.

The influence of the phase nonreciprocity on the self-starting laser was experimentally studied both in IAP RAS (Nizhny Novgorod) and Imperial College (London). The results were the same.

The experiments showed that generation threshold, energy of generated pulses and average power depend on the cavity phase nonreciprocity. The generation threshold can be decreased and generation power can be increased by using phase nonreciprocity (Fig. 6.4).

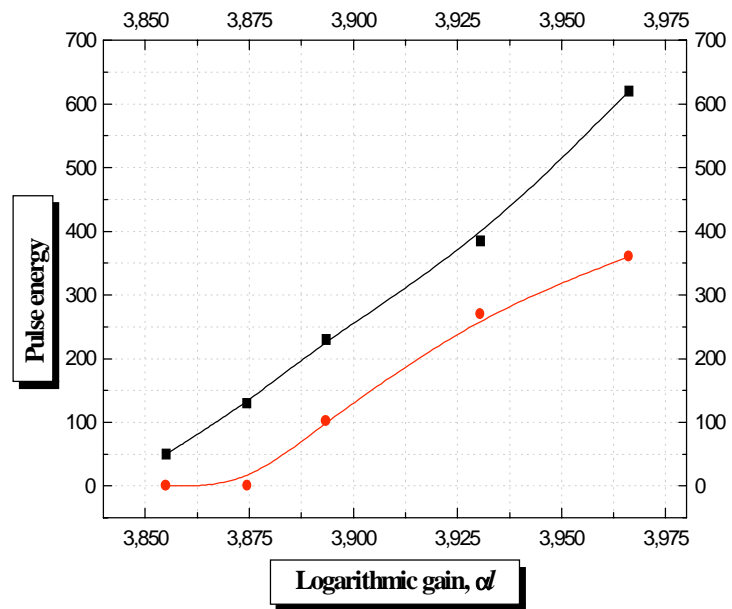


Fig. 6.4. Measured generated pulse energy vs gain of the Nd:YAG amplifier in the laser with the dynamic cavity with phase nonreciprocity “ -0.5π ” (black line) and “ 0.5π ” (red line).

In conclusion, our study showed the influence of the phase nonreciprocity of the cavity of a self-starting laser on its generation threshold and output power. This fact should be taken into account in analyzing different schemes of the self-starting lasers.

7. Investigation of mode-locking in self-starting laser with dynamic cavity.

We studied the self-starting laser with cavity completed by dynamic grating induced in media with fast nonlinearity. A saturable absorber based on a polymethine dye in a polyurethane matrix with picosecond relaxation time was used as the nonlinear medium [14]. New cells with polymer films 100...300 μm in thickness placed between two glass plates were used in these experiments. Motivation for this study was the search for a new method of self-mode-locking using self-starting lasers with dynamic cavity.

7.1. Self-starting laser with a non-Bragg multi-grating nonlinear mirror

The most interesting result was obtained in the scheme with multi-intersecting waves in the nonlinear layer (Fig. 7.1). The thickness of the nonlinear layer was 100 μm , and the intersection angle was the same (about 0.1 rad) for all three pairs of waves. Non-Bragg diffraction on the holographic gratings in the thin layer provided the interaction of the intersecting waves due to higher diffraction orders. The use of the dye-doped polymer layer both as a dynamic holographic medium and a convention saturable absorber enabled generation of a pulse train with sub-nanosecond single-pulse duration.

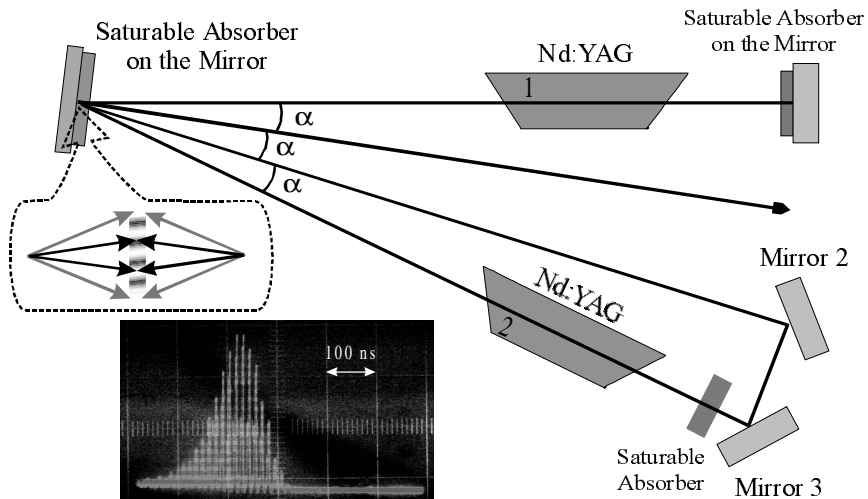


Fig. 7.1. Schematic of the self-starting laser with a non-Bragg nonlinear mirror in the saturable absorber, wave-vector diagram and oscillosogram of the generated pulse train.

The temporal behavior of the pulse train slightly varied from one pump pulse to another. The most regular dynamics of the generated pulse train was registered near the self-starting oscillation threshold (Fig. 7.2b).

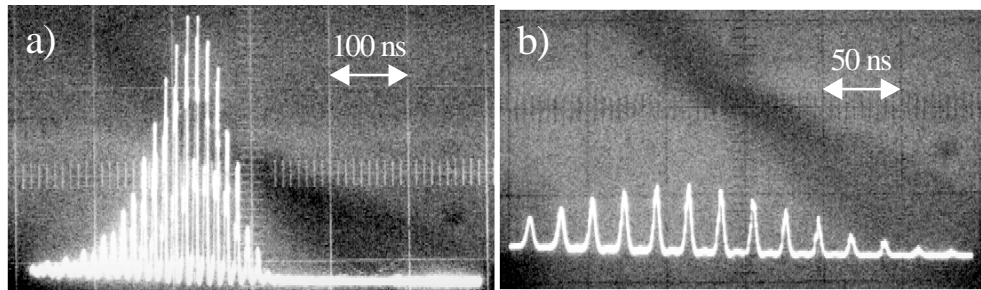


Fig. 7.2. Oscillosograms of the output beam in the self-starting laser with the fast nonlinear mirror far above oscillation threshold (a) and near threshold (b).

The total energy of the pulse train consisting of 10...30 pulses was measured to be up to 10 mJ.

Dynamics of each pulse of the generated train was also studied using a fast oscilloscope scale. Pulses far above generation threshold demonstrated a rather complicate temporal behavior (Fig. 7.3). The train dynamics and each pulse temporal structures indicated that far above generation threshold we have a finite number of the locking modes. In other words, we have partially mode-locking pulses.

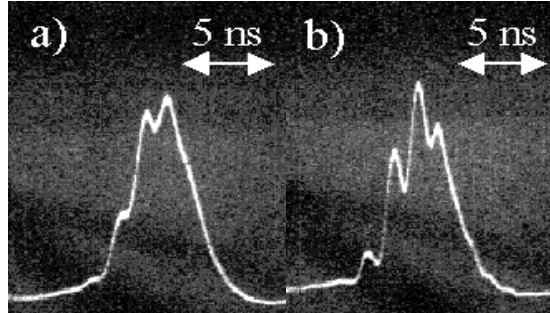


Fig. 7.3. Oscillosgrams of the generated pulses in the train far above the self-starting oscillation threshold.

7.2. Mode-locking in laser with a double-phase conjugate mirror in the fast nonlinear absorber

In the next series of our experiment, a laser scheme with a transmitting dye-doped polymer layer was studied. Two optical waves intersected in the nonlinear layer and induced a transmitting grating of population in the saturable absorber. This grating completed the cavity by reflecting the intersection waves from one direction to another. The nonlinear layer played the role of a nonlinear double-phase conjugated mirror. To avoid any small-scale reflection grating, which could decrease the spectral bandwidth of the generation beams, we used an additional 90° polarization rotator (PR) in the cavity.

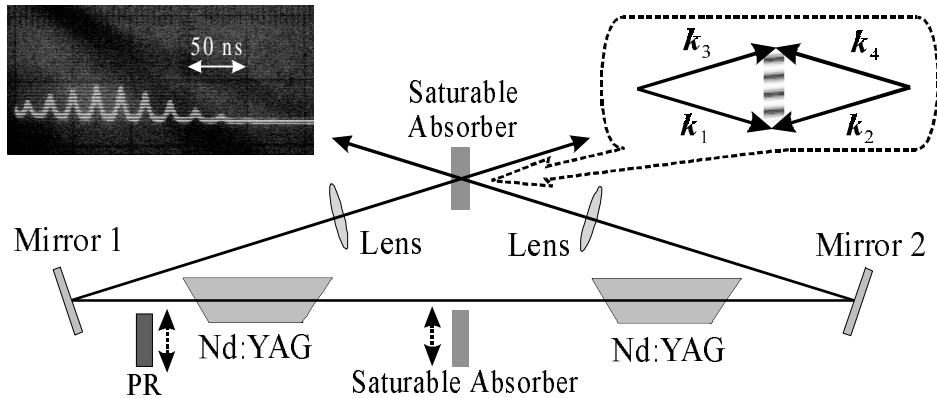


Fig. 7.4. Schematic of the laser with a double-phase conjugate mirror, wave-vector diagram and oscillosgram of the mode-locking pulse train.

Generation threshold of the laser with the double-phase conjugate mirror was found to be much higher than for the single-output cavity; however, the mode-locking regime was achieved more easily.

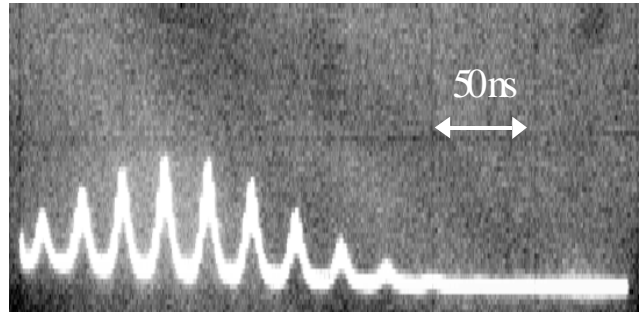


Fig. 7.5. Dynamics of the generated pulse train in the double output scheme.

The mode-locking generation was obtained by use of lenses with the focal distance of 25...28 cm. The measurement of pulse duration in the train was made by the well-known FROG method (second harmonic generation in the intersection area of two mutually-delayed parts of the beam). For this purpose, an additional amplifier of the generated pulses was used. This measurement indicates the characteristic pulse duration of about 30...100 ps. Unfortunately, the generation is limited due to degradation of the polymer (within 20-30 minutes of operation with the pulsed laser even at \sim 1-Hz repetition rate) resulting in optical breakdown of the film. The most serious problem in the experiment was the degradation of the polymer film and its optical breakdown.

When the focal distance of at least one lens was increased to 50 cm the picosecond mode-locking generation was absent. In this case, generation of pulses with duration of several nanoseconds or several tens of nanoseconds was recorded. The former generation (i.e. pulses at several nanoseconds) can be explained by partial mode-locking, while the latter generation (pulses with several tens of nanoseconds) – by self-Q-switching. These regimes are caused by the thermal grating formed in the absorbing polymer. This thermal grating with period of about 10 μ m having decay time in polymer of about 20 μ s is integrated during several round trips through the cavity, leading to the long-pulse generation.

Therefore, our experiments have confirmed the possibility in principle of the mode-locking generation in the Nd:YAG laser with dynamic cavity completed by a fast- relaxed grating which plays a role of broadband nonlinear dynamics mirror. A disadvantage of the investigated self-starting laser is low damage threshold of the dye-doped polymer saturable absorber. However, this technique can be used for other active and nonlinear media to obtain reliable mode-locking generation.

8. Experimental investigation of the high average power laser

The investigation of the possibility for obtaining high-average power beam with good quality in the self-starting Nd:YAG laser with dynamic cavity was one of the main goals of the project. Several experimental schemes of the laser with adaptive cavity were studied to achieve this goal.

8.1. A “8-like” scheme of the self-starting laser.

An 8-like architecture of self-starting laser was investigated (Fig. 8.1, and reports 2 and 3 [8,10]). The scheme comprises two Nd:YAG rods of big sizes (dimensions of rods 1 and 2 were 12×135 mm^2), mirrors, and polarization elements (Fig. 8).

The energy of the generated pulse train with a repetition rate of \sim 30 Hz reached 8.0...9.0 J. It gives about 240...270 W of average power. However, the output beam quality was not good. The beam-quality parameter was $M^2 \approx 9 \dots 10$. The use of additional polarization rotators (90° polarization quartz rotators and a Faraday rotator) did not provide any considerable improvement of the beam quality.

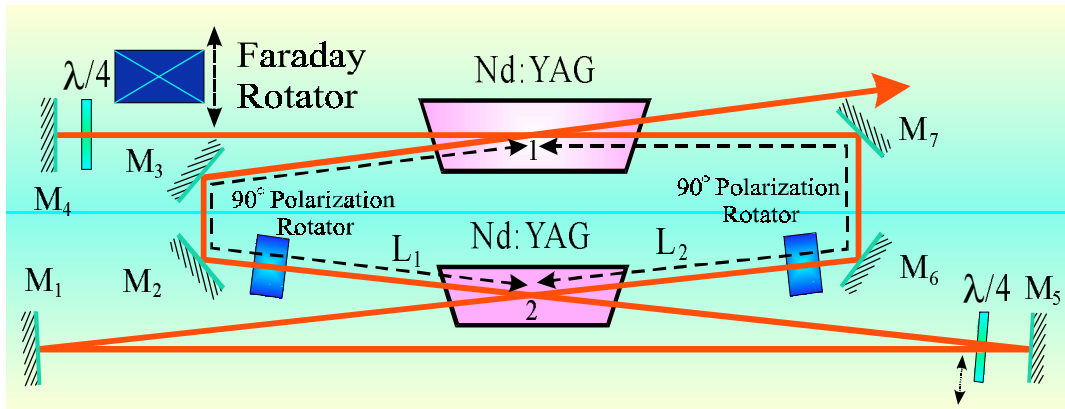


Fig. 8.1. The schematic of a self-starting laser includes two Nd:YAG rods, two polarization rotators, mirrors (M_1 - M_7), and quarter-wavelength plates ($\lambda/4$) or a Faraday rotator.

8.2. A “simple” scheme.

In this scheme the number of optical elements was decreased. It comprises two Nd:YAG rods of big sizes (dimensions of rods 1 and 2 were $12 \times 135 \text{ mm}^2$), lenses F_1 and F_2 , mirrors and a polarization rotator (Fig. 8.2). The lenses F_1 and F_2 , along with the summed thermal lens of the two rods, give telescopes, thereby minimizing diffraction losses in the scheme. For compensation of polarization aberrations in the rods a 90° polarization quartz rotator (placed between two flash-lamp-pumped Nd:YAG rods) was used.

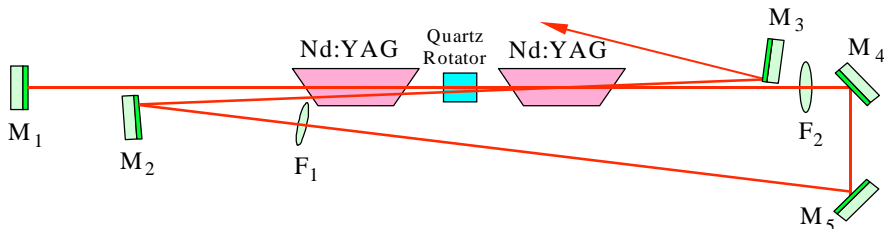


Fig. 8.2. A new variant of the self-starting scheme comprising 2 Nd:YAG rods, and lenses F_1 and F_2 .

The experimental results were as follows: a) generation of a beam with average power up to 100...120 W was achieved; b) the generated beam quality was not good ($M^2 > 5...8$). The disadvantages of this scheme are as follows: 1). imperfect quality of the generated beam, which again may be explained by strong polarization distortions not totally compensated by simply rotating the polarization; 2). decrease in the average power of the generated beam in comparison with other scheme.

8.3. The scheme with telescope imaging transfer

To improve the depolarization compensation, another scheme was devised. This scheme comprises two Nd:YAG rods of big sizes (dimensions of rods 1 and 2 were $12 \times 135 \text{ mm}^2$), 5 lenses, mirrors, and a quartz rotator (Fig. 8.3). This scheme utilizes the idea of compensation of thermally induced birefringence by transferring images of the principle plane of one amplifier rod to the principle plane of another rod and by rotating the beam polarization at 90° [15].

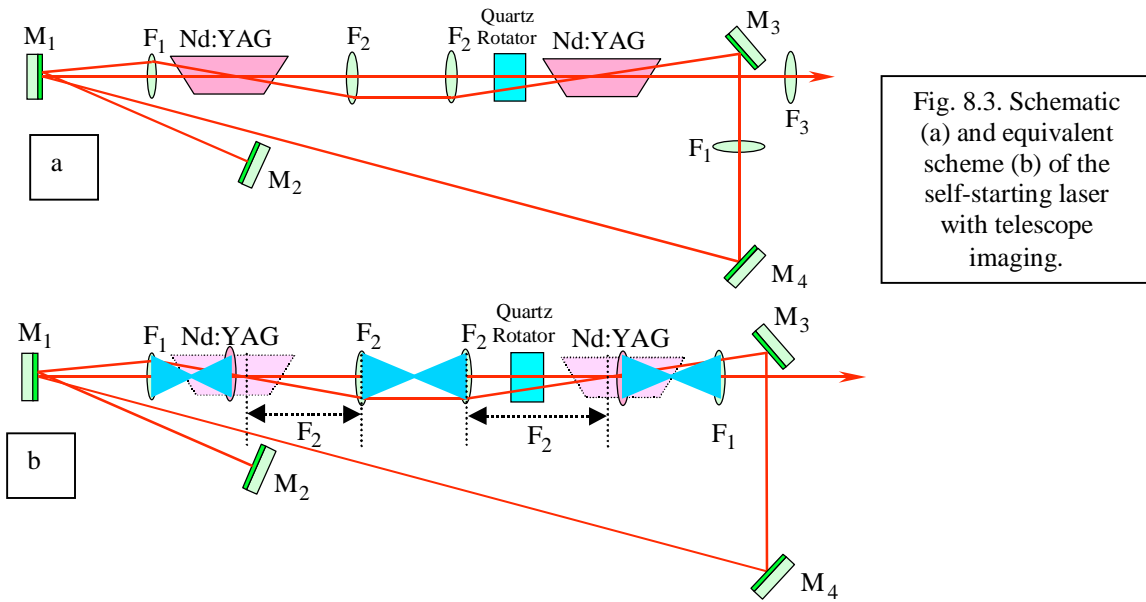


Fig. 8.3. Schematic (a) and equivalent scheme (b) of the self-starting laser with telescope imaging.

The results of our experimental study of this scheme are as follows. A beam with good quality can be obtained (M^2 was estimated close to 1). However, the average power of the generated beam is still small (of about 50...60 W), which is likely to be due to strong diffraction losses on the big total lens of the cavity that was about 12 m.

8.4. “Compact” scheme with image transfer

At the next step of our investigation, the self-starting laser with compact cavity and image transfer was realized (Fig. 8.4. and see report 4). This scheme comprises two Nd:YAG rods with big sizes (\varnothing 12 mm, and length of 135 mm), several lenses, mirrors, and a quartz rotator.

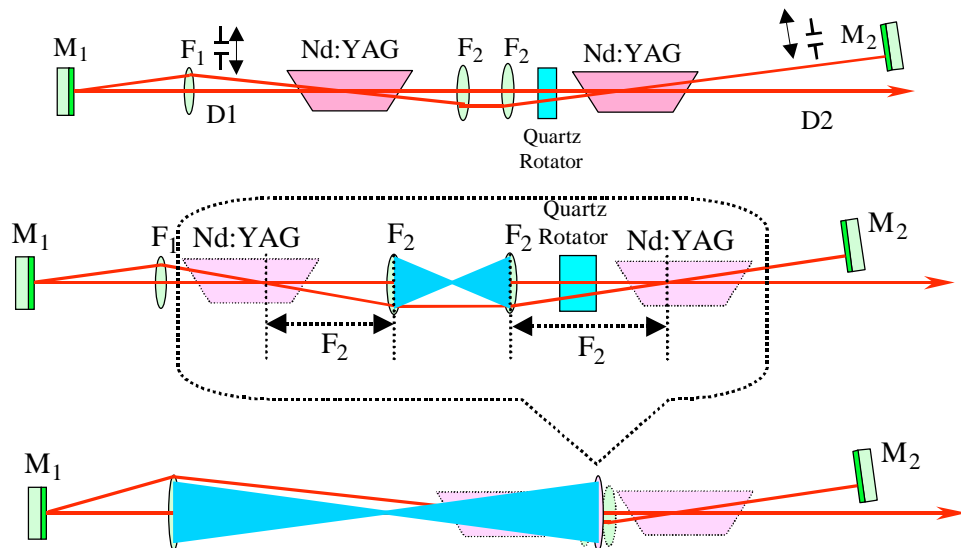


Fig. 8.4. Schematic and equivalent scheme of the self-starting laser with telescope imaging: F_1 - F_2 - lenses; M_1 and M_2 - mirrors; Nd:YAG - amplifiers.

We again try to realize the idea of compensation of thermally induced birefringence by transferring images of the principle plane of one amplifier rod to the principle plane of another rod and by

rotating the beam polarization at 90°. This method is good for two identical amplifier rods.

The experiment was directed at optimization of the scheme by appropriately choosing lenses and cavity distances. The equivalent cavity has a small length (about 180 cm).

The influence of intracavity diaphragms (D1, D2) on beam quality and average power was also investigated (Table 8.1.). The output average power of 290...300 W with beam quality $M_x^2 = 2.96$, $M_y^2 = 3.80$ was experimentally obtained.

Table 8.1.

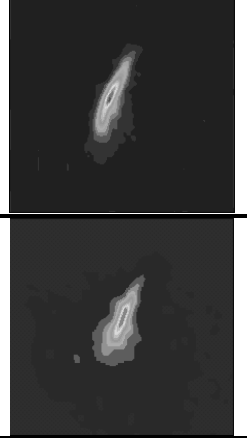
D2, mm	5	4	3	2	
D1, MM					
2.7	2.6	2.5	2.2	2.1	M_x^2
	2.2	1.4	1.6	2.4	M_y^2
	254 W	225 W	205 W	185 W	
3	2.7	2.3	2.2	1.9	M_x^2
	2.9	2.2	2.3	2.5	M_y^2
	259 W	244 W	215 W	200 W	
-	2.9	2.3	1.02	1.2	M_x^2
	2.8	2.3	2.0	1.9	M_y^2
	283 W	264 W	234 W	211 W	

The analysis of the beam power and quality showed its high sensitivity to the diameter of the diaphragm D₂ placed in the backward-reflecting arm of the scheme. For understanding of the selective property of the laser the Fresnel parameter of an equivalent scheme was calculated. The beam quality was found to be a function of the Fresnel parameter (Table 8.2). The good beam quality at average power more than 250W was obtained for the effective Fresnel number of about 2...3. This generation was stable in time. This fact indicates good adaptive property of the dynamic cavity. Indeed, a Nd:YAG laser with common mirrors and the similar Fresnel number is unable to generate a good-quality beam. Similar result was obtained in our previous study of the self-starting laser based on the Nd:YAG rods of small dimensions ($\varnothing 6 \times 100$ mm and $\varnothing 10 \times 100$ mm) [...].

The experiments showed that the quality of the generated beam in the plane of the scheme was higher than in the orthogonal plane. This result can be explained by better selectivity of the dynamic holograms in the plane of the beam intersection.

Table 8.2.

Diameter of diaphragm D2	Fresnel Parameter	Average Power	Beam Quality	Transversal Intensity Distribution (far field)
5 mm	3.25	283 W	$M_x^2 = 2.7$ $M_y^2 = 2.9$	
4 mm	2.08	264 W	$M_x^2 = 2.1$ $M_y^2 = 2.7$	

3 mm	1.17	234 W	$M_x^2 = 1.02$ $M_y^2 = 2.0$	
2 mm	0.52	211 W	$M_x^2 = 1.2$ $M_y^2 = 1.9$	

Therefore, the last variant of the self-starting laser has demonstrated a possibility of generation of the high-average-power beam with good quality. This scheme appears to be quite simple and reliable. It has additional potential for power increase by use of an additional pass, the three-dimensional architecture can give an improvement of beam quality (or semitransition of the beam).

The investigated scheme can be used in a diode-pumped laser system. However, now it is clear that the nonlinearity of the flash-lamp-pumped Nd:YAG crystal and the diode-pumped crystal is quite different. Therefore, the diode-pumped self-starting laser requires further investigation.

9. References

1. O.L. Antipov, A.S. Kuzhelev, D.V. Chausov, and A.P. Zinov'ev, "Dynamics of refractive index changes in a Nd:YAG laser crystal under Nd³⁺-ions excitation," *J. Opt. Soc. America B*, vol. **16**, pp. 1072-1079, 1999.
2. O.L. Antipov, A.S. Kuzhelev, A.Yu. Luk'yanov, A.P. Zinov'ev, "Changes in the refractive index of an Nd:YAG laser crystal on excitation of the Nd³⁺ ions", *Quantum Electronics*, v. **28**(10), pp. 867-974 (1998).
3. A.A. Kaminskii, B.M. Antipenko, "Multilevel Functional Crystal Laser System" (Moscow: Nauka, 1989).
4. X.S. Bagdasarov, I.S. Volodina, A.I. Kolomiychev, M.L. Meylman, A.G. Smagin, "Spectrum characteristics of Nd:YAG in UV and visible range", *Sov. Quan. Electron.* **9**, N. 6, pp. 1158-1166 (1982). (Rus.)
5. M.A. Kramer, and R.W. Boyd, "Three-photon absorption in Nd-doped yttrium aluminum garnet", *Phys. Rev. B* **23**, pp. 986-991 (1981).
6. G.V. Venikouas, G.J. Quarles, J.P. King, and R.C. Powell, "Spectroscopy of Nd:YAG under high-power picosecond-pulse excitation", *Phys. Rev. B* **30**, pp. 2401-2409 (1984).
7. Richard C. Powell, "Physics of Solid-State Laser Materials" (Springer-Verlag, New York-Berlin-Heidelberg, 1998), p. 327.
8. The Third Report To European Office of Aerospace Research and Development "Self-starting solid-state laser with dynamic self-adaptive cavity", Submitted to EOARD at August 10, 2001.
9. The First Report To European Office of Aerospace Research and Development "Self-starting solid-state laser with dynamic self-adaptive cavity", Submitted to EOARD at February 10, 2001.
10. The Second Report To European Office of Aerospace Research and Development "Self-starting solid-state laser with dynamic self-adaptive cavity", Submitted to EOARD at May 20, 2001.
11. M.J. Damzen, R.P.M. Green, and K.S. Syed, "Self-adaptive solid-state oscillator formed by dynamic gain-gratings holograms," *Opt. Lett.* **20**, 1704-1706 (1995).
12. O.L. Antipov, A.S. Kuzhelev, and D.V. Chausov, "Formation of the cavity in a self-starting high-average power Nd:YAG laser oscillator," *Opt. Express* **5**, 286-292 (1999).

13. S.G. Odulov, M.S. Soskin, A.I. Khizhnyak, "Dynamic grating lasers," Moscow: Nauka (1990).
14. V.I. Bezrodnyi, A.A. Ishchenko, L.V. Karabanova, Yu.L. Slominskii "Highly stable polymethine-dye-based polymer switches for passive mode locking in neodymium laser", *Quant. Electr.* **22**, N 8, pp. 849-852, 1995.
15. Q. Lu, N. Kugler, H. Weber, S. Dong, N. Muller, and U. Wittrock, "A novel approach for compensation of birefringce in cylindrical Nd:YAG rods," *Opt. Quantum Electron.*, **28**, pp. 57-69, 1996.
16. O.L. Antipov, D.V. Chausov, A.S. Kuzhelev, V.A. Vorob'ev, A.P. Zinoviev, "250W-Average-Power Nd:YAG Laser with Self-Adaptive Cavity Completed By Dynamic Refractive-Index Gratings", *IEEE Quantum Electronics*, v. **37**, issue 5, pp. 716-724 (May 2001).
17. O.L. Antipov, A.S. Kuzhelev, V.A. Vorob'ev, A.P. Zinoviev, "Milisecond pulse repetitive Nd:YAG laser with self-adaptive cavity formed by population gratings," *Opt. Comm.*, v. **152**, pp. 313-318, 1998.

II. PRESENTATIONS OF THE RESULTS

Published Papers

1. O.L. Antipov, D.V. Chausov, A.S. Kuzhelev, A.P. Zinoviev, "Self-starting laser oscillator with a nonlinear nematic liquid crystal mirror", *JOSA B* **18**, N1, pp. 13-20 (2001).
2. O.L. Antipov, D.V. Chausov, A.S. Kuzhelev, V.A. Vorob'ev, A.P. Zinoviev, "250W-Average-Power Nd:YAG Laser with Self-Adaptive Cavity Completed By Dynamic Refractive-Index Gratings", *IEEE Quantum Electronics*, v. **37**, issue 5, pp. 716-724 (May 2001).

Presentations at Conferences and in Technical Digests

3. O.L. Antipov, A.S. Kuzhelev, D.V. Chausov, "High average-power self-starting Nd:YAG laser with cavity completed by self-induced refractive index gratings", Conference on Lasers and Electro-Optics Europe (Nice, France, September 2000), Conference Digest, CTuN2, p.154
4. A.P. Zinov'ev, A.S. Kuzhelev, O.L. Antipov, "Self-starting phase-conjugate laser with dynamic liquid-crystal holographic mirror", Conference on Lasers and Electro-Optics Europe (Nice, France, September 2000), Conference Digest, CTuN4, p.155.
5. O.L. Antipov, A.V. Afanas'ev, D.V. Chausov, A.S. Kuzhelev, V.A. Vorob'ev, and A.P. Zinoviev, "300W-average-power Nd:YAG laser with self-adaptive cavity completed by dynamic holographic gratings", in *OSA Trends in Optics and Photonics (TOPS)* vol. 56, Conference on lasers and Electro-Optics (CLEO 2001), Technical Digest, Postconference Edition (Optical Society of America, Washington DC, 2001), CWH2, pp. 341-342.
6. O.L. Antipov, A.P. Zinoviev, D.V. Chausov, and A.S. Kuzhelev, "Self-starting Nd:YAG laser oscillator with a ring cavity formed by a resonant double-phase-conjugate mirror", in *OSA Trends in Optics and Photonics (TOPS)* vol. 56, Conference on lasers and Electro-Optics (CLEO 2001), Technical Digest, Postconference Edition (Optical Society of America, Washington DC, 2001), CThL41, pp. 465-466.
7. O.L. Antipov, A.V. Afanas'ev, O.N. Eremeykin, A.P. Zinov'ev, V.A. Gur'ev, O.S. Morozov, A.P. Savikin, "Excited-state absorption and population of higher-lying levels of Nd³⁺ ions under diode and laser pumping of Nd:YAG crystals", Technical Digest of XVII International Conference on Nonlinear Optics "ICONO" 2001, Minsk, Belarus, June 26 - July 1, 2001, p. 253, paper FP26.
8. O.L. Antipov, A.P. Zinoviev, D.V. Chausov, A.V. Afanas'ev, "Self-organization of nonlinear dynamic cavity in a high-average-power laser oscillator", Technical Digest of XVII International Conference on Nonlinear Optics "ICONO" 2001, Minsk, Belarus, June 26 - July 1, 2001, p. 225, paper FJ1.

9. O.L. Antipov, O.N. Eremeykin, V.A. Vorob'ev, A.P. Savikin, I.F. Nurgaleev, A.S. Samborsky, "The excited state absorption in Nd:YAG crystal under laser and diode pump", Technical Digest of 2 International Conference of Young Scientists "Optics – 2001", p. 47 (2001).
10. O.L. Antipov, A.V. Afanas'ev, D.V. Chausov, A.S. Kuzhelev, V.A. Vorob'ev, and A.P. Zinoviev, "300W-average-power Nd:YAG laser with self-adaptive cavity completed by dynamic holographic gratings", in OSA Trends in Optics and Photonics (TOPS) vol. **56**, Conference on Lasers and Electro-Optics (CLEO 2001), Technical Digest, Postconference Edition (Optical Society of America, Washington DC, 2001), CWH2, pp. 341-342.
11. O.L. Antipov, A.P. Zinoviev, D.V. Chausov, and A.S. Kuzhelev, "Self-starting Nd:YAG laser oscillator with a ring cavity formed by a resonant double-phase-conjugate mirror", in OSA Trends in Optics and Photonics (TOPS) vol. 56, Conference on lasers and Electro-Optics (CLEO 2001), Technical Digest, Postconference Edition (Optical Society of America, Washington DC, 2001), CThL41, pp. 465-466.
12. O.L. Antipov, D.V. Chausov, A.P. Zinoviev, "Cavity architectures and dynamics of self-starting laser oscillator with nonlinear mirror", Technical Digest of CLEO-Europe Focus Meeting "Progress in Solid-State Lasers" (18-22 June 2001), paper C-PSL-148, p. 148 (2001).
13. O.L. Antipov, A.V. Afanas'ev, O.N. Eremeykin, A.P. Zinov'ev, "Excited state absorption and formation of dynamic gratings in diode pumped Nd:YAG crystals", Technical Digest of CLEO-Europe Focus Meeting "Progress in Solid-State Lasers" (18-22 June 2001), paper C-PSL-130, p. 130 (2001).
14. A.P. Zinov'ev, O.L. Antipov, "Mode locking in a self-starting laser with cavity completed by fast holographic grating", in OSA Trends in Optics and Photonics (TOPS) vol. 73, Conference on lasers and Electro-Optics (CLEO 2002), Technical Digest, Postconference Edition (Optical Society of America, Washington DC, 2002), CMA5, pp. 4-5.
15. D.V. Chausov, O.L. Antipov, "Influence of phase nonreciprocity on self-starting oscillator with cavity formed by population grating", in OSA Trends in Optics and Photonics (TOPS) vol. 73, Conference on lasers and Electro-Optics (CLEO 2002), Technical Digest, Postconference Edition (Optical Society of America, Washington DC, 2002), CMA6, pp. 5-6.
16. A.P. Zinov'ev, O.L. Antipov, G.E. Yudakin, "Mode locking in a self-starting laser with cavity completed by fast population grating", Technical Digest of International Quantum Electronics Conference (IQEC2002), Moscow, Russia, June 22-27, 2002, paper QsuR41, p. 121.
17. O.L. Antipov, O.N. Eremeykin, V.A. Vorob'ev, A.P. Savikin, "Fluorescence spectroscopy and interferometric measurement of refractive index change of Nd:YAG laser crystal under intensive diode pumping", Technical Digest of International Conference on Laser, Applications and Technologies (LAT2002), Moscow, Russia, June 22-27, 2002, paper LME18.

III. Purchase of the equipment

The QCW laser diode stack at 808 nm with peak power up to 300W (type SPL QY81K) was purchased by ISTC in "Opto Semiconductors" Corporation, Germany. The device has been received by ISTC in June 2002.

IV. Budget report

Money was spent for Individual Financial Support:

O.L. Antipov	\$ 10,500,
A.P. Zinov'ev	\$ 3,440,
D.V. Chausov	\$ 2,520,
A.V. Afanas'ev	\$ 700,
V.A. Vorob'ev	\$ 1,080,
O.N. Eremeykin	\$ 1,720,
I.V. Yurasova	\$ 360,
L.G. Kozina	\$ 500,
A.P. Savikin	\$ 1,150,
I.F. Nurgaleev	\$ 100,
A.S. Samborskii	\$ 100,
N.A. Markelov	\$ 100.

SubTotal: \$ 22,270.00

Laser diode Array SPL QY81K 9,525.00 EURO (\$8,448.00)

TOTAL 30,718.00

Principal Investigator:



/Oleg Antipov/